MASTER THESIS

Neuronal and Synaptic Organization of Layer 1
in the Human Temporal Lobe Neocortex:
A Quantitative Electron Microscopic Analysis

A thesis submitted by

JULIA STÖHR

University of Applied Sciences Hamburg
Faculty Life Sciences
Pharmaceutical Biotechnology

Research Centre Jülich GmbH
Institute of Neuroscience and Medicine (INM-2)
Molecular Organization of the Brain
Group: 'Structure of Synapses'

First supervisor: Prof. Dr. Oliver Ullrich
Second supervisor: Prof. Dr. Joachim HR Lübke

August 2017

TABLE OF CONTENTS

1 INTRODUCTION

1.1 THE HUMAN NEOCORTEX

The largest and evolutionary newest part of the mammalian and hence the human brain is the cerebral cortex consisting of 20-40 billion neurons. The neocortex (isocortex) represents the largest part of the cerebral cortex in humans, although it is a very thin layer of 2-4mm thickness (Kandel et al., 2013). One of the most characteristic features of the cerebral cortex in higher mammals, in particular in primates, is the highly increased surface area, and thus the volume, by deep grooves (sulci) and ridges (gyri) (Ronan et al., 2014) allowing more space to integrate more neurons. Roughly, the neocortex is composed of a grey matter containing distinct types of neurons, their dendrites and axons terminating in synapses that altogether form the intrinsic and extrinsic network of the neocortex. The in- and output structure of the neocortex is called the white matter because of ascending and descending myelinated axons, which send information from the neocortex towards the sensory periphery and vice versa.

Although evolutionary young, the neocortex is the region of the brain, in which higher-order brain functions like sensory perception, cognition, sophisticated motor control, spatial reasoning and language take place (Lui et al., 2011; Lodato and Arlotta, 2015). The most characteristic and fundamental feature of the neocortex (isocortex) is its organization into six layers, namely Layer 1 to Layer 6 apart from granular cortices that lack a prominent Layer 4. Other important features of the neocortex are so-called vertically oriented columns, fundamental functional building blocks (Mountcastle et al., 1957; Mountcastle and Powell, 1959; Hubel and Wiesel, 1963) and a discontinuous system of long-range horizontal axons (Horton and Adams, 2005; Lübke and Feldmeyer, 2007).

Each cortical column of the neocortex contains ~15.000 to ~20.000 neurons throughout all layers. About ~80% of these neurons are excitatory (glutamatergic), while the remaining ~20% are various types of inhibitory (GABAergic) interneurons (Noback et al., 2005). While

the excitatory neurons, namely pyramidal cells and spiny stellate neurons, constitute the output system of the neocortex, GABAergic interneurons serve as the feedforward and feedback inhibitory system that controls and modulates the excitatory neurons by highly target-specific local or widespread inhibition. Every neuron receives about ~10.000 to ~15.000 synaptic contacts distributed over the entire dendritic tree of the target neuron.

The temporal lobe (TL) neocortex represents ~17% of the cerebral cortex in humans (Kiernan, 2011), and exhibits a more 'complex' cytoarchitecture regarding its thickness, larger neurons (Mohan et al., 2015), density of synaptic contacts per neuron (DeFelipe et al., 2002; 2011) and the composition of the astrocytic network than that observed in rodents and monkeys (Elston et al., 2001; DeFelipe, 2011). Because the TL neocortex is a typical and thus representative example of a granular, six-layered neocortex such as the somatosensory and visual neocortex described in humans (von Economo and Koskinas, 1925; Zilles et al., 2015), it became attractive for structural and functional investigations. Hence TL epilepsy is one of the most frequent types in humans, neocortical non-affected (non-epileptic) access tissue becomes available during surgery.

1.2 Layer 1 of the Human Temporal Lobe

Layer 1 (L1) in the adult neocortex is regarded as a cell sparse layer containing only a small, but very heterogeneous, population of GABAergic interneurons (Wozny and Williams, 2011; Muralidhar et al., 2013; Jiang et al., 2016), terminal tuft dendrites from pyramidal neurons in L2/3, L5 and L6 (reviewed by Marin-Padilla, 1975) and non-neuronal cells, namely astrocytes and oligodendrocytes. In addition, L1 contains axonal collaterals from several excitatory and inhibitory neurons, spiny stellate, pyramidal neurons, and L1 (local) and L1 projecting interneurons (Wang et al., 2004b) and is thus regarded as an important 'commissural and associational fiber' layer.

In contrast to its adult appearance, L1 plays a significant role in the development of the neocortex which starts with the proliferation of stem (progenitor) cells into neuron and glial cells building the ventricular and marginal zone (MZ) that later becomes L1. Thus, L1 is beside the so-called subplate, a transient cell layer, the first layer to be established.

In a timely sequence excitatory neurons are generated in the ventricular zone and migrate tangentially along radial glia (Meyer and González-Gómez, 2017), following the insight

first-outsight last-principle in the establishment of cortical layers in the cortical plate (Luskin and Shatz, 1985; 1986). The majority of GABAergic interneurons originates from the so-called lateral and medial ganglionic eminence (reviewed by Wonders and Anderson, 2006; Ma et al., 2013) and from there migrate into their prospective cortical target layers.

Since L1 is one of the first layers to be generated, neurons in L1 are among the first born and migrating in the neocortex. Beside GABAergic interneurons form so-called Cajal-Retzius (CR) cells, originating from different places of birth (Bielle et al., 2005), a dense and long-range horizontal network in L1 during development including a high density of synaptic boutons along their axons. This dense network of CR cells is thought to have a major impact on the development of cortical columns providing an excitatory 'drive' required to anchor terminal tuft dendrites of pyramidal neurons and to place neurons in their prospective target layer under the control of the lipoprotein *reelin* (reviewed by D'Arcangelo, 2001; Ogawa et al., 1997). After the establishment of the six-layered structure of the neocortex CR cells underlie caspase 3-driven apoptotic cell death and are completely disappeared during the third postnatal week in the neocortex (Anstötz et al., 2014).

1.3 THE STRUCTURE OF SYNAPSES

The term 'synapse' (from Greek synapsis "conjunction", from synaptein "to clasp", from syn- "together" and haptein "to fasten") was introduced more than 100 years ago in 1897 by the famous English physiologist Charles Sherrington. This term was later adopted by the famous neuroanatomist Ramon ý Cajal, although the synapse was not structurally identifiable at that time (Carlos and Borrell, 2007).

Synapses are the key elements in the induction, maintenance and termination of signal transduction between neurons in any given network of the brain. Most nerve-to-nerve and all known nerve-to-muscle and nerve-to-gland signaling rely on chemical synapses at which the presynaptic neuron releases a chemical neurotransmitter that acts on the postsynaptic target neuron (Lodish et al., 2013). Per definition, a synapse (synaptic contact) is composed of three structural elements at the pre- and postsynaptic apposition zone: the presynaptic end terminal, the synaptic cleft and the postsynaptic target structure that could be a soma, dendrite or spine. The pre- and postsynaptic densities together with the synaptic cleft form the so-called active zone (AZ). The axon terminus of the presynaptic cell, the so-called synaptic bouton, contains

several hundreds or thousands of synaptic vesicles, numerous mitochondria, and a cocktail of various synaptic proteins that constitute the presynaptic density (reviewed by Südhof, 2012). This assembly of synaptic proteins (for example the SNARE complex) regulates the mobilization, transportation, priming, docking and fusion of synaptic vesicles under the control of internal calcium. Each of the vesicles contains either an excitatory or inhibitory neurotransmitter, in the neocortex glutamate and y-aminobutyric acid (GABA) are the main neurotransmitters. Evoking a single or multiple action potentials at the synaptic bouton triggers the fusion of a single or multiple synaptic vesicle. After opening, a single or multiple quanta of neurotransmitter are released and diffuse via the synaptic cleft, a structure that contains so-called fuzzy material and is between 20 to 50nm in widths. The diameter of the cleft critically determines the diffusion of neurotransmitter molecules (quanta) and hence the efficacy of a synapse (reviewed by Xu-Friedman and Regehr, 2004; Neher, 2015). The postsynaptic element could be either a soma of a neuron, a dendrite or spine. The postsynaptic density is the recipient zone of the neurotransmitter or various neuromodulator substances composed of highly specialized neurotransmitter receptors and proteins involved in various postsynaptic signal cascades (reviewed by Südhof, 2012).

Both excitatory and inhibitory synapses are highly target specific. Synaptic contacts are established between axons and proximal and distal dendrites (axo-dendritic), dendritic spines (axo-spinous), somata (axo-somatic) and exclusively with the axon initial segment (axo-axonic contact) of the target neuron.

To further categorize synapses Gray (1959) postulated two different types of CNS synapses according to structural differences at the electron microscopic (EM) level: so-called Gray Type 1 synapses typically found on dendritic shafts and spines defined by a prominent postsynaptic density of various shape and size. In contrast, Gray Type 2 synapses also innervate dendritic shafts but also somata and are characterized by a less prominent or lack of postsynaptic density. These two types were later referred to as asymmetric (excitatory) and symmetric (inhibitory) synapses (Colonnier, 1968) and could be further distinguished by the shape and diameter of their synaptic vesicles: excitatory synaptic boutons have larger, more round synaptic vesicles, while in inhibitory terminals vesicles are smaller and more oval shaped.

This target-specific innervation, the density, distribution pattern together with the balance and ratio of excitatory and inhibitory synapses on their prospective postsynaptic target neuron modulates and regulates the computational properties of any given neuron and consequently their network performance in a given brain region.

1.4 IDENTIFICATION OF SYNAPTIC STRUCTURES

As already stated above, the term ‘synapse’ was already introduced in the 19th century. Due to the work of Ramon ý Cajal and Camillo Golgi, the two leading neuroanatomists at that time, it became possible for the first time to visualize neurons in great detail in different brain structures. This lead to a revolution and fundamental new insights in brain architecture (Glickstein, 2014), the work of Ramon ý Cajal on the structural organization of the brain (1911) is still a standard work in cellular neuroscience.

The light microscope uses passing visible light transmitted from the specimen, which is bundled via several optical lenses to generate an image that can be inspected at various magnifications. Although the light microscope opened a new window in the description of various aspects of brain structure and connectivity, it has severe limitations: the final magnification is up to 1500-fold and the resolution is limited by 0.2µm (Wilson and Bacic, 2012), as the most important property of any microscope is not the magnification but the resolution (Lodish et al., 2013). Moreover, only strong reflecting objects can be imaged and the clarity is reduced by diffraction light being out of focus.

A revolution in the structural identification of synapses was the introduction of an electron microscopic lens in 1926 by Busch. The first electron microscopic prototype was built by the physicist Ernst Ruska and the electrical engineer Max Knoll in 1931.

The beam of an EM at high-voltage (around 80-120kV) emits accelerated electrons by a filament as a source of illumination and is focused by electromagnetic lenses through an ultra-thin specimen. Objective and projector lenses focus the electrons passing the sample and project them onto a viewing screen or camera. Since atoms in air absorb electrons, the entire system from filament (electron source) to the detector maintains under an ultrahigh vacuum (Lodish et al., 2013).

EM can generate a resolution up to 0.1nm and a maximum magnification of x1,000,000 that nowadays allows high-end fine-scale structural investigations at the cellular, subcellular and molecular level. Since then, and in particular since the decade of the brain, EM became an important tool in the investigation of various aspects of brain architecture and organization.

1.5 AIM OF THE THESIS

Using a broad spectrum of different techniques including state-of-the-art molecular, electrophysiological, high resolution, fine-scale light-, confocal, single- and two photon, electron force and modern EM imaging has steadily improved our knowledge about synaptic structures. This enabled new insights to structure and function of brain microcircuits and network properties in different brain regions and thus finally improved our understanding of the computational properties in the normal adult, developing and pathologically altered brain.

Although meanwhile numerous publications have described various aspects of synaptic structures in great detail, our knowledge about the quantitative geometry of these structures is still limited to a relatively small number of central nervous system (CNS) synapses in various animal species and brain regions (for example: hippocampal subregion CA1 (Harris and Stevens, 1989; Harris and Sultan, 1995; Schikorski and Stevens, 2001; Marrone et al., 2005; Nava et al., 2014), hippocampal mossy fiber boutons (Chicurel and Harris, 1992; Rollenhagen et al., 2007; reviewed by Rollenhagen and Lübke, 2010; Wilke et al., 2013), cerebellar climbing fiber synapses (Xu-Friedman et al., 2001); the cochlear bushy cell synapse and calyx of Held synapse (Nicol and Walmsley, 2002; Sätzler et al., 2002; Wimmer et al., 2006; Hoffpauir et al., 2007; Müller et al., 2009), cerebellar mossy fibers (Xu-Friedman and Regehr, 2003), the ribbon synapse in the retina (Sikora et al., 2005) and neocortical synapses (Rollenhagen et al., 2014; Dufour et al., 2016; Bopp et al., 2017; Hsu et al., 2017).

In contrast, comparatively little is known about synapses in humans, in particular no coherent and comprehensive studies exist (but see for example: Alonso-Nanclares et al., 2008; Navarrete et al., 2013; Mohan et al., 2015; DeFelipe et al., 1999; 2011) which is partially attributable to the availability of tissue with an excellent ultrastructural preservation. It turned out, that human samples from post-mortem brains are not suitable for fine-scale and hence quantitative analysis of synaptic structures due to severe structural alterations. To overcome this problem, we have taken advantage of tissue samples derived from patients that underwent epilepsy surgery (for details see Chapter 2). This approach results in excellent ultrastructural preservation and hence allows the quantification of several structural parameters that represent structural correlates for synaptic transmission and plasticity.

The aim of the master thesis was several-fold:

1) The description of the structural organization of L1 in the human TL neocortex
2) The quantitative analysis of structural subelements of synaptic boutons in L1
3) The generation of quantitative 3D models of L1 synaptic boutons
4) The comparison of the quantification between synaptic boutons located in two regions of L1

This is achieved using a combination of high-end, fine-scale EM and subsequent computer-assisted three-dimensional (3D) volume reconstruction based on digital EM images. This work will contribute to an improved understanding of the 'behavior' of synapses embedded in different networks of the human brain.

2 MATERIAL AND METHODS

All experimental procedures were approved by the Ethical Committees of the Rheinische Friedrich-Wilhelms-University/University Hospital Bonn (ethic votum of the Medical Faculty to Prof. Dr. med. J. Schramm and Prof. Dr. rer. nat. Joachim Lübke, Nr. 146/11), the University of Bochum (ethic votum of the Medical Faculty to Dr. Marec von Lehe and Prof. Dr. rer. nat. Joachim Lübke), the Research Committee of the Research Centre Jülich GmbH and complied with the guidelines laid out in the EU directive regarding the work with human tissue used for experimental and scientific purposes (2004/23/EC).

2.1 MATERIAL AND PATIENT SELECTION

In this work biopsy material of two female patients, aged 37 and 43, suffering from TL epilepsy was investigated (Table 1). The neocortical brain tissue collected during epilepsy surgery derived from pharmaco-resistant patients. The pre-surgery work included frequent high-resolution MRI and long-term-video-EEG-monitoring. In both cases the epileptic focus was located and restricted in the hippocampus proper leaving the surrounding neocortex unaffected (non-epileptic). Tissue blocks of the neocortex were sampled from the access material, being remote from the epileptic focal region, which was resected to control the seizures and for subsequent histological inspection. Results of the histopathological examination displayed no structural abnormalities. Therefore, the sampled biopsy material can be regarded as ‘normal’ with respect to the structural composition.

Table 1: Patient Information
Additional information about patients of selected biopsy material, like gender, age and tissue region of access material.

Identity	Gender	Age [years]	Histopathological result	Tissue Region
HU_160217	Female	43	Ganglioglioma	TL (right)
HU_110204	Female	37	Ganglioglioma	TL (left)

The samples (tissue blocks), used in this study, were taken from biopsy material of either the left or right TL, mainly from various locations of the Gyrus temporalis medialis or inferior temporal gyrus (Table 1).

2.2 TISSUE FIXATION AND PROCESSING FOR 3D RECONSTRUCTION

Directly after sample collection during epilepsy surgery small tissue blocks were immediately immersion-fixed in ice-cold phosphate buffered (PB) 4% paraformaldehyde and 2.5% glutaraldehyde (Fixation Buffer, see Table 2) for 24-48 hours at 4°C. Fixation buffer was changed twice during the fixation period. After multiple washing steps (3x5min) with cold PB, the tissue was cut into 150 or 200µm thick vibratome sections (VT1000S Leica Microsystems, Nussloch, Germany) at the frontal (coronal) plane through the human neocortex. Slices were collected in multiwell plates in PB. After thorough washing in cold PB (3x5min), sections were post-fixed for 90min in osmium tetroxide (Table 2) at room temperature in the dark. After several rinses in PB (5x10min), slices are covered with small round glass plates to prevent deformation of the sections during the following dehydration. Sections were incubated for 10min each in an ascending series of ethanol (20%, 30%, 40%, 50%, 60%, 70%, 80%, 90%), followed by 30min in 95% ethanol and twice 30min in absolute ethanol. Subsequently sections were transferred from multiwell plates into small glass flasks and briefly washed (2min twice) in propylene oxide (Fluka, Neu-Ulm, Germany). Slices were then incubated in a mixture of Durcupan® and propylene oxide (1:2 for 1 hour, 1:1 for 1 hour) and afterwards stored in pure resin overnight. For polymerization sections were embedded in fresh Durcupan® on coated glass slides or between acla-foil at 60°C for 2-3 days.

The embedded osmium-treated sections (Figure 3A) were examined under a light microscope (Olympus BX61) and were documented using the Olympus CellSense software (Olympus GmbH, Hamburg, Germany). An area of interest was cut out and glued on a pre-polymerized block. Semithin sections with a thickness of 1µm were cut and stained with methylene blue (Figure 3B-C) and a second smaller and more defined area of interest, inside the first, was selected under the light microscope.

Table 2: Composition of Chemical Solutions used for Sample Preparation
Chemical components and composition of solutions used during tissue fixation and processing for semithin- and ultrathin sectioning.

Solution	**Component**	**Concentration/ Mass**
Fixation Buffer pH 7.4	Phosphate buffer Paraformaldehyde Glutaraldehyde	0.1M 4% 2.5%
Osmium-Fixative pH 7.4	Phosphate buffer Sucrose Osmium tetroxide (Sigma, Munich, Germany)	0.1M 0.646% 0.5 to 1%
Durcupan® (Durcupan C is not added before mixture of A, B and D are homogenous)	Durcupan A Durcupan B Durcupan C Durcupan D (Fluka, Neu-Ulm, Germany)	100g 100g 1g 3g
Methylene Blue Stain	Methylene Blue Aqueous Azur II	(1:1)
Lead Citrate	Lead nitrate Sodium citrate Aqua bidest	1.76g 1.33g 30ml

Serial ultrathin sections (43-55nm, silver to grey interference color) were cut through the area of interest with a diamond knife (Ultracut Leica Microsystems, Nussloch, Germany) and transferred onto a Pioloform coated copper slot grid (Figure 1A-D). Prior to EM examination, sections were stained with 5% aqueous uranyl acetate for 15-20min and lead citrate for 3-5min according to Reynolds (1963) to enhance the contrast of biological membranes at the EM level.

The series of ultrathin sections of patient HU_160217 consisted of 87 and that of patient HU_110204 of 71 individual ultrathin sections on copper coated grids.

The ultrathin series were investigated using a Zeiss Libra 120 EM (Carl Zeiss Microscopy, Oberkochen, Germany) equipped with a bottom-mounted slow scan 2K Proscan digital camera and the corresponding ImageSP analysis software (Albert Tröndle, Moorenweis, Germany). In the first series of ultrathin slices two regions of interest (ROI) were selected. For the reconstruction, regions with well-preserved synaptic structures and dendrites were taken for further quantitative analysis. Furthermore, by the definition of a ROI the difficulty of tracing the selected area had to be taken into consideration to guarantee the right consistency. The first ROI was selected being close to the pial surface and glia limitans within L1a (Figure 3B-C). An area deeper in L1, close to the L1/L2 border (Figure 3B), was selected as a second ROI in L1b. The defined two ROI (22x22µm) were photographed at a primary magnification x8000 (frame size 6x6 images/ROI) through the entire series.

Additional pictures of various regions within L1 were taken for further documentation and illustration at different magnifications.

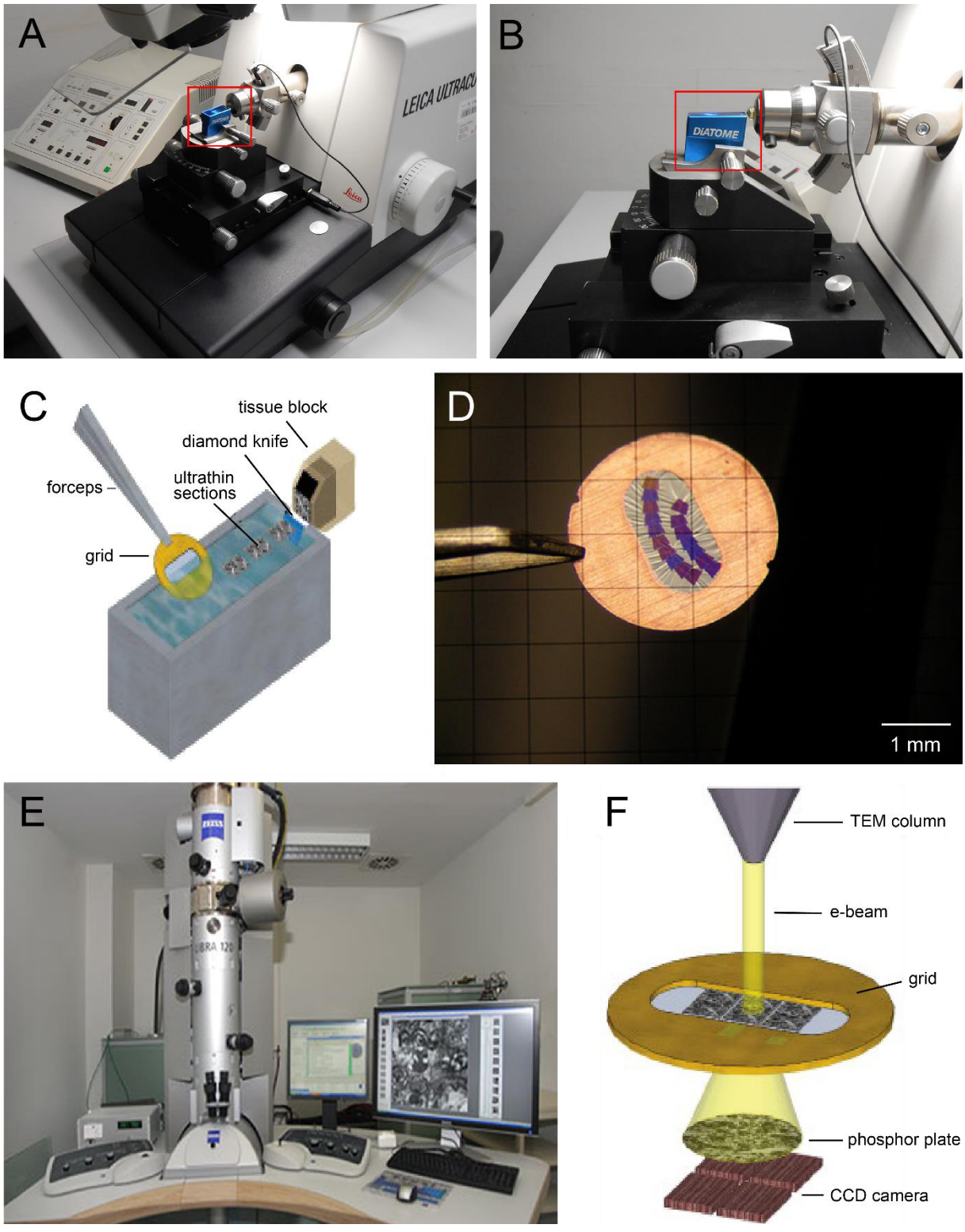

Figure 1: Preparation of Ultrathin Sections and electron microscopic Examination
A) Ultrathin sectioning with Leica Ultracut. **B)** Magnified side view of the block holder and diamond knife (red framed area). **C)** Schematic illustration of ultrathin sectioning procedure. Ultrathin sections from block cutting float free on water and are collected onto a Pioloform coated copper slot grid. **D)** Pioloform coated copper grid with two rows of ultrathin sections. Thickness of ultrathin sections is indicated by the interference contrast (silver to grey appearances). **E)** Electron microscope (Zeiss Libra 120) equipped with a bottom mounted 2K slow Proscan digital camera and computer hard- and software for data acquisition, storage and analysis. **F)** Schematic illustration of electron microscopic operation. (Images: with courtesy from Rachida Yakoubi).

2.3 3D VOLUME RECONSTRUCTION

For reconstruction, all serial images of one ROI were imported into the reconstruction software OpenCAR (Sätzler et al., 2002). Individual digital EM images were stacked and linearly transformed such, that corresponding structures were aligned along all consecutive images comprising the 3D image stack. Synaptic structures of interest were determined by contouring in different defined colors (Figure 2). After outlining synaptic structures of interest in all images throughout the series, subsequent 3D volume reconstructions and space-limited tables were generated by OpenCAR.

To guarantee a preferably correct reconstruction only complete synaptic structures that could be followed from the beginning to the end in consecutive digital images were analyzed. Two types of synaptic boutons were distinguished for 3D volume reconstruction: *Endterminal boutons*: the axon of the synaptic bouton could be followed through the entire series of ultrathin sections. The termination was defined by the diminishment until the structure was too small to be tracked. The second type of boutons were so-called *En-passant-boutons*: here, the axon leading to a bouton could be followed in both directions in consecutive images.

The reconstructions were made using an offline batch version of OpenCAR that allowed the quantification of surface area and volume of the selected structures (Synaptic boutons, mitochondria, active zones, synaptic- and dense-core vesicles) and diameters (synaptic and dense-core vesicles).

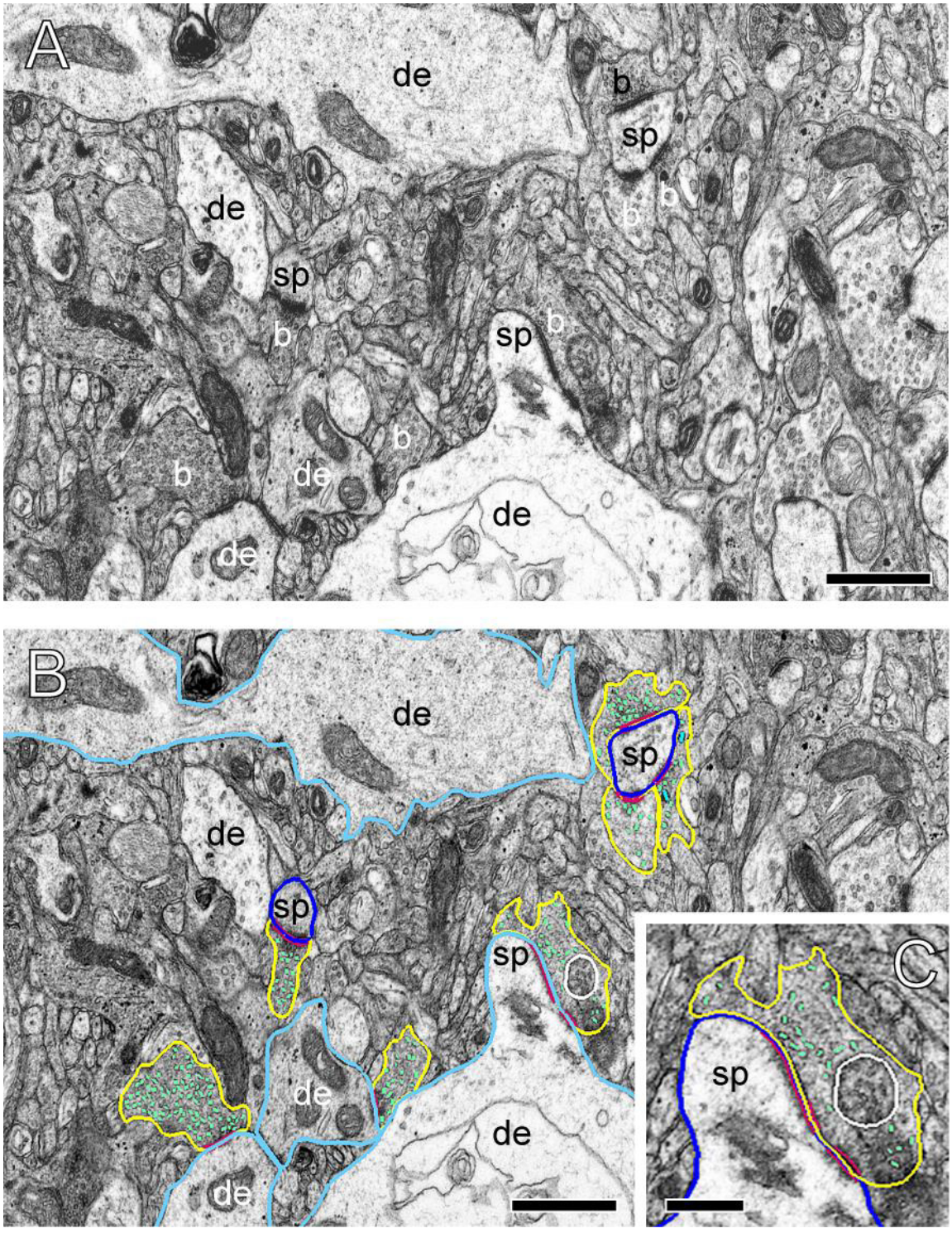

Figure 2: Quantitative Reconstruction of Synaptic Structures using Software OpenCAR
A) Cut out of a high power digital 6x6 frame EM image using the panorama multi alignment function of the ImageSP software. In these images structures of interest were reconstructed by contouring. For better visualized identification, synaptic structures have been marked as follows: synaptic boutons (b), dendrites (de), spines (sp). **B)** Same image as shown in A. Here, synaptic structures of interest were outlined by contours. Color code: Synaptic boutons (yellow), dendrites (light blue), spines (dark blue), mitochondria (white), pre- and postsynaptic AZs (red) and synaptic vesicles (green). Scale bars in A and B 500nm. **C)** The inset shows a higher magnification of the contouring of a synaptic bouton. Note the green marked diameter of the vesicles. Scale bar 250nm.

2.4 Quantitative Analysis of the Structural Synaptic Parameters

It has to be mentioned that the quantitative analysis of the huge amount of data as produced here is very labor-intensive and hence time-consuming and needs absolute accuracy. Nevertheless, as a first step surface area and volume of the synaptic boutons, the volume of mitochondria and the total number of synaptic vesicles per synaptic bouton was estimated to allow the definition of the total vesicle pool. In addition, the synaptic vesicle diameter and the total synaptic vesicle volume were determined. Moreover, the distance of each vesicle to the presynaptic density was calculated for the estimation of the three functionally defined vesicle pools. Finally, the number and size of dense core vesicles were analyzed. They often appear twice in consecutive sections due to their greater diameter and were hence counted in the image when they appeared largest.

The quantitative analysis of the size of the AZ (structural equivalent to the functional transmitter release site) is not part of the master thesis, but will be performed in the PhD thesis. This is also the case for the definition of the three pools of synaptic vesicles, namely the readily releasable (RRP), the recycling (RP) and resting pool (Rizzoli and Betz, 2005).

2.5 Statistical Analysis of the Structural Synaptic Parameters

The 3D volume reconstructions in OpenCAR provided the basis for the subsequent quantitative analysis. First, the spreadsheets generated by OpenCAR were summarized for every patient and region of interest to calculate different structural parameters (see above). A box plot analysis (Figure 11) revealed no significant differences between the two patients; hence the obtained data were pooled together. The results of the quantitative analysis are expressed as means with the corresponding standard deviation (see Chapter 3.4).

For further evaluation, the median with the 1st and 3rd quartile and the correlation coefficients (R^2) were generated. The non-parametric Kruskal-Wallis H-test with Dunn's post-hoc analysis was used to look for variances between the different defined regions of interest (L1a and L1b) and human samples for the structural parameters analyzed. P-values are given where appropriate and $p<0.05$ was considered significant.

3 RESULTS

In this study, biopsy material of L1 of the human TL neocortex has been qualitatively and quantitatively investigated. A total of 60 synaptic boutons have been reconstructed and analyzed.

3.1 STRUCTURAL ORGANIZATION OF LAYER 1

The human TL is a typical example of a granular, six-layered neocortex as identified in methylene blue stained semithin sections (Figure 3B-C) and hence comparable to other neocortical regions of the human brain, like the visual and the somatosensory cortex (von Economo and Koskinas, 1925; Zilles et al., 2015).

Since relatively little is known about the structural, in particular the synaptic organization of L1 in humans, this layer became the focus of this Master thesis.

In humans, L1 occupies a comparably large volume of the neocortex (Figure 3A, C) as visualized in methylene blue stained and in EM micrographs (Figures 3 and 4). In both micrographs, L1 is seen as the first cortical layer located underneath the three meninges, from which the pia mater is directly attached to the cortical surface (Figure 3B-C). The pia mater consists of a thin fibrous connecting tissue also containing numerous blood vessels and fibroblasts.

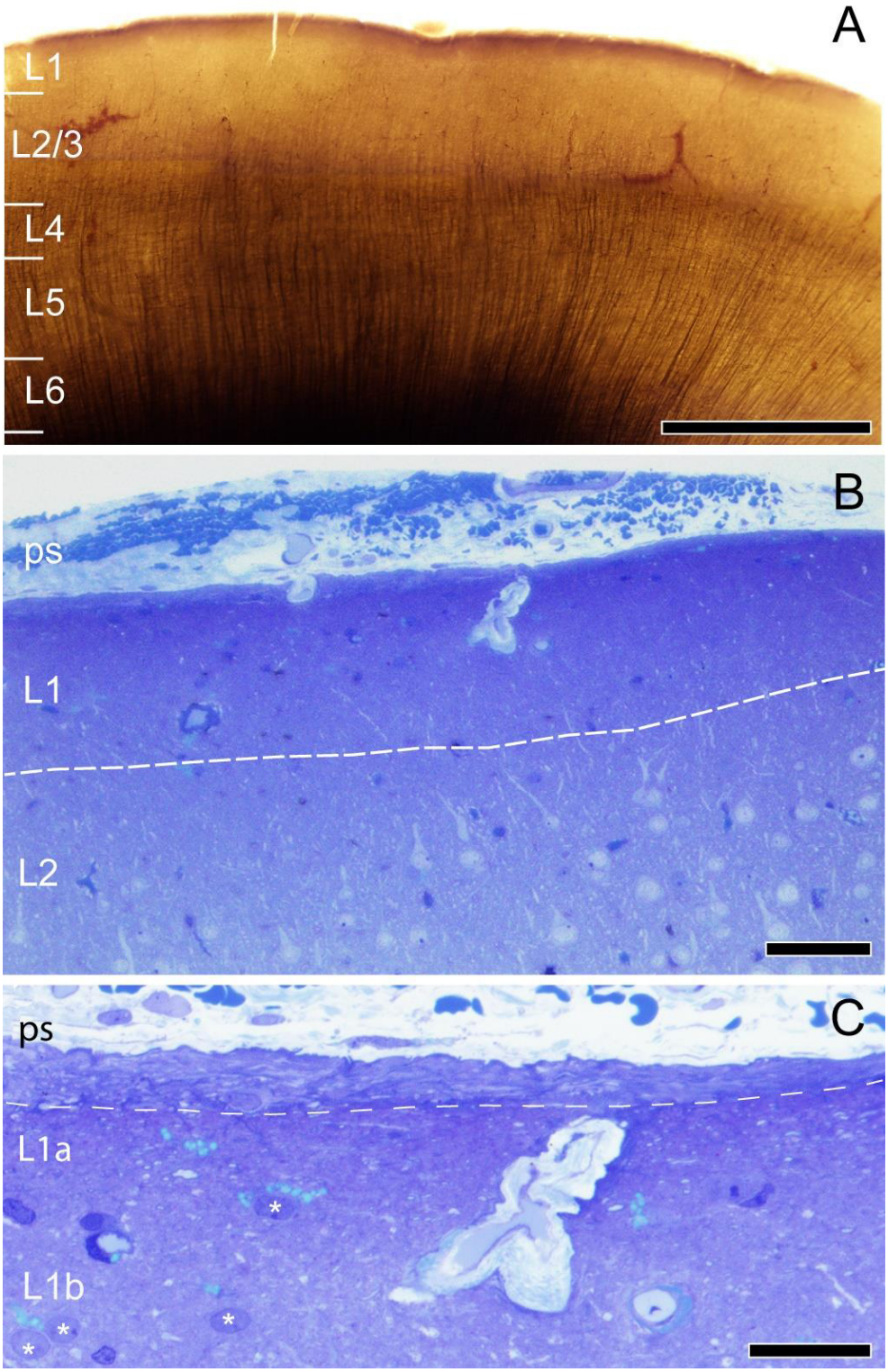

Figure 3: Preparation of Blocks and semithin Sectioning

A) Low power light micrograph of an osmium tetroxide treated vibratome section with a thickness of 100µm. Bars indicate borders of L1 to L6 of the grey matter of the neocortex. Scale bar 1mm. **B)** High power semithin methylene blue stained section trough spinal pia mater (ps) and L1 and L2. Dashed line marks the border between L1 and L2. Note the transition from the cell sparse (L1) to a cell rich layer (L2) containing numerous neurons and dendrites. Scale bar 50µm. **C)** Same image as in B at a higher magnification showing only L1. Dashed line marks the imaginative border between the glia limitans and L1, asterisks indicate neurons. Scale bar 20µm.

Underneath the pial surface astrocytic end foot processes spreading from both perivascular and marginal astrocytes form a close association with the basal lamina of the parenchyma to create the glia limitans (Figure 3C, 4A). Within this dense network of astrocytic processes small caliber elongated dendrites of different shape and size formed by terminal tuft dendrites of L2/3, L5 and L6 neurons were observed (Figure 4A, C). L1 can easily be identified by the glia limitans as the upper part and the abrupt increasing high density of pyramidal and non-pyramidal cells of L2 as lower border. Hence, L1 in human was subdivided in sublamina L1a and sublamina L1b (Figure 3C).

In the adult human neocortex, L1 is characterized by the low density of cells, including neuronal and non-neuronal types, compared to the deeper layers of the neocortex (compare Figure 3B with 3C). L1 consists of numerous GABAergic interneurons, identifiable by their nuclear infoldings, and glia cells (Figure 5C) along with apical dendrites of pyramidal cells of the underlying layers (Marin-Padilla and Marin-Padilla, 1982). Interestingly, a characteristic feature of the human neocortex are persistent CR cells that in contrast to animal species survive and do not undergo selective caspase 3-driven cell death (Figure 4C). Numerous GABAergic interneurons and CR cells show so-called lipofuscin granular within their cytoplasm (Figure 5A, B), a characteristic feature in aged neurons. The CR cell in Figure 5B established a so-called axon initial segment (AIS), which emerged from the soma to create synaptic contacts with synaptic boutons. An AIS can be defined by the neurofilament within the tangle (Inset of Figure 5B).

The non-neuronal components in L1 (macroglia system) are astrocytes and oligodendrocytes. Astrocytes and their fine processes were observed reaching throughout the entire L1, with a high degree of fine astrocytic processes in the glia limitans and directly below (Figure 4A). In general, astrocytes (Figures 4A, B and 5C) are known to serve as a ‘skeleton’ stabilizing the neuropil around neurons and as nutrient suppliers. However, in the CNS astrocytes play a key role in synaptic transmission and plasticity structurally forming a so-called tripartite synapse. This complex is composed of a synaptic bouton, its target structure and the surrounding astrocytic processes. In L1 a tight ensheathment of fine astrocytic processes with synaptic complexes was observed, however, not yet quantified. Randomly we observed synaptic contacts between fine astrocytic processes and synaptic boutons (Figure 7F).

In addition to astrocytes, numerous oligodendrocytes were found throughout L1 often associated with myelinated and unmyelinated axons (not shown) suggesting that they are still in the process of producing and forming the myelin sheath around axons.

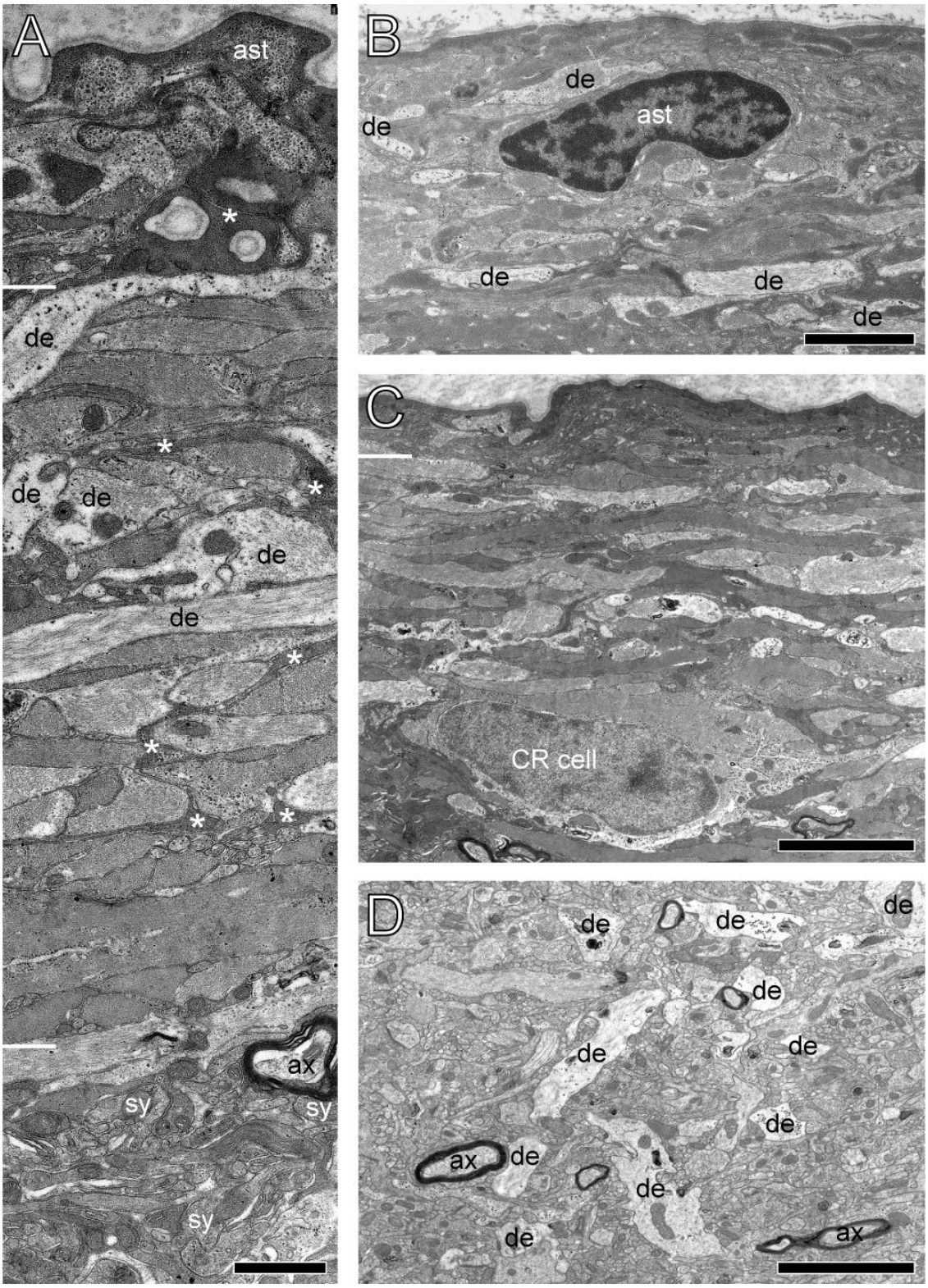

Figure 4: Overview of Layer 1 in the Temporal Lobe Neocortex

A) Electron micrograph of upper L1: bars separate pial surface and underneath lying glia limitans, upper dendritic zone, first region with high density of synaptic contacts. Astrocyte (ast) and astrocytic processes (asterisks) are typical for this region. High density of horizontal dendrites (de) is followed by region with many synaptic contacts (sy) and axons (ax). Scale bar 1µm. **B)** Astrocyte (ast) close to the pia surrounded by horizontal dendrites (de). Scale bar 2µm. **C)** CR cell close to the pial surface. Scale bar 3µm. **D)** Lower dendritic zone characterized by dendrites (de) surrounded by myelinated axons (ax). Scale bar 2µm.

Occasionally, gap junctions have been observed between diverse types of cells, for example between astrocytes and interneurons (Figure 5C) but also between CR cells and neighboring astrocytes (not shown). Gap junctions are characterized by the typical three-layered structure (inset Figure 5C) and serve as cell-to-cell contacts that allow the diffusion of various molecules, including amino acids, nucleotides, second messengers and ions through these contacts. In addition, also electrical signals can pass through these junctions (Lampe and Lau, 2004).

In summary, L1a is characterized by the glia limitans with fine astrocytic processes, small caliber elongated terminal tuft dendrites and several but rare synaptic boutons (Figure 4A). In addition, also cells bodies of astrocytes, (Figure 4B), oligodendrocytes, CR cells (Figure 4C, 5A-B) and GABAergic interneurons (Figure 5C) were found.

In contrast to the structural composition of L1a, the most striking difference in L1b is the abruptly increasing and high density of synaptic boutons (Figure 4A) and the occurrence of larger caliber dendrites of different shape (Figure 4C). These dendrites that give rise to the terminal tuft dendrites seen in L1b are sometimes organized in clusters of dendrites (Figure 4D) forming so-called dendrons.

In summary, L1b represents the more ‘dendritic domain’ of L1. To look for possible differences in the composition of synaptic boutons they were quantitatively analyzed in both sublaminae.

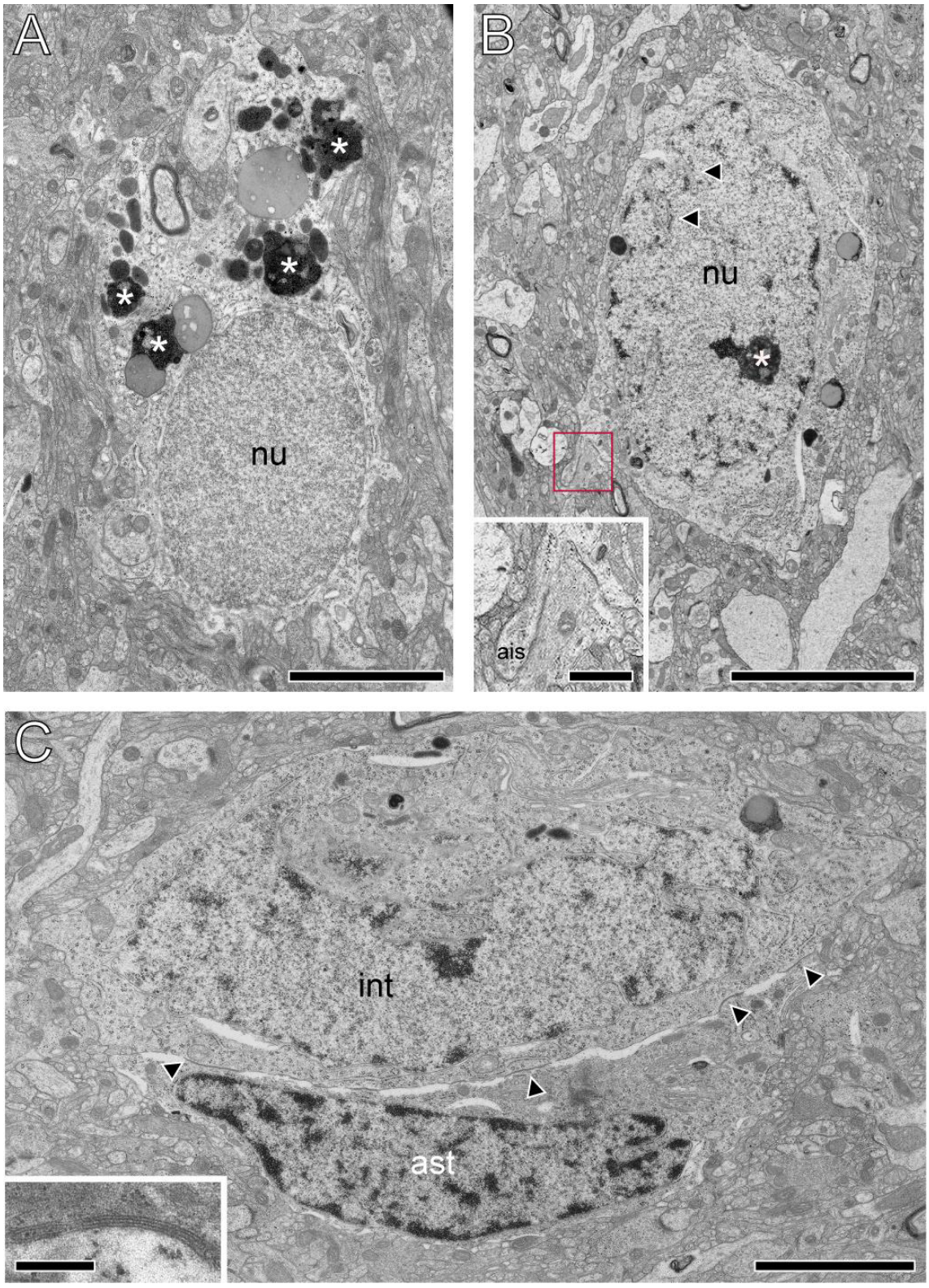

Figure 5: Neuronal Composition of Layer 1

A) Typical CR cell showing a dislocated nucleus (nu) with incorporations, so-called lipofuscin granula, throughout their cytoplasm (marked as asterisk). Scale bar 3µm. **B)** CR cell with typical nuclear infoldings (arrowheads) and large nucleus (nu). Axon initial segment (ais) with neurofilaments (red frame and inset) Scale bar 5µm. Inset: scale bar 500nm. **C)** GABAergic interneuron (int) in close proximity to an astrocyte (ast). Arrowheads mark gap junctions between soma of interneuron and astrocyte. Scale bar 2µm. **Inset** shows higher magnification of gap junction characterized by a three-layered structure. Scale bar 250nm.

3.2 QUALITATIVE SYNAPTIC ORGANIZATION OF LAYER 1

At the subcellular level, the neuropil of L1 contains a dense network of synapses and their target structures, mainly ascending dendrites of L2/3 and L5 pyramidal cells and a dense network of astrocytes and their fine processes.

Each synaptic complex is composed of a synaptic bouton and a target structure, which can be a dendritic shaft (Figure 7A), a dendritic spine of different shape and size (Figure 6), the soma of a neuron or an AIS (Figure 5B). Dendritic spines can be further distinguished into stubby spines (Figure 6A, C), mushroom spines (sometimes elongated) (Figure 6B-D) and filopodial spines (Figure 6E). The majority of spines (~70%) contained a so-called spine apparatus (Figure 6B-C), a derivate of the endoplasmic reticulum. It is thought that spines containing a spine apparatus are more mobile and hence modulate short- and long-term synaptic plasticity (Deller et al., 2003; Konur and Yuste, 2004; Umeda et al., 2005). Most synaptic boutons (~70%) were observed to establish a single synaptic contact with a dendrite or a spine, while ~23% established two synaptic contacts with one or two target structures. The remainder, mainly those of much larger size, were found to share three to four synaptic contacts with one or more target structures. Furthermore, a highly specialized form of synapse so-called dendro-dendritic synapses (Figure 7C) and a small number of synapses between astrocytes and synaptic boutons (Figure 7F) were infrequently observed.

The majority of synaptic boutons were glutamatergic, indicated by a prominent postsynaptic density and comparably large, round vesicles, while GABAergic synaptic terminals (see Chapter 1.3) were only frequently found located on dendritic shafts and somata, but also on dendritic spine but rarely.

The majority of presynaptic boutons contained mitochondria (Figure 6A,Figure 7D) and clear synaptic vesicles, of which some are ~2-3 fold larger, the so-called dense core vesicles (Figure 7D) and two membrane specializations, the pre- and postsynaptic densities which together with the synaptic cleft form the AZ.

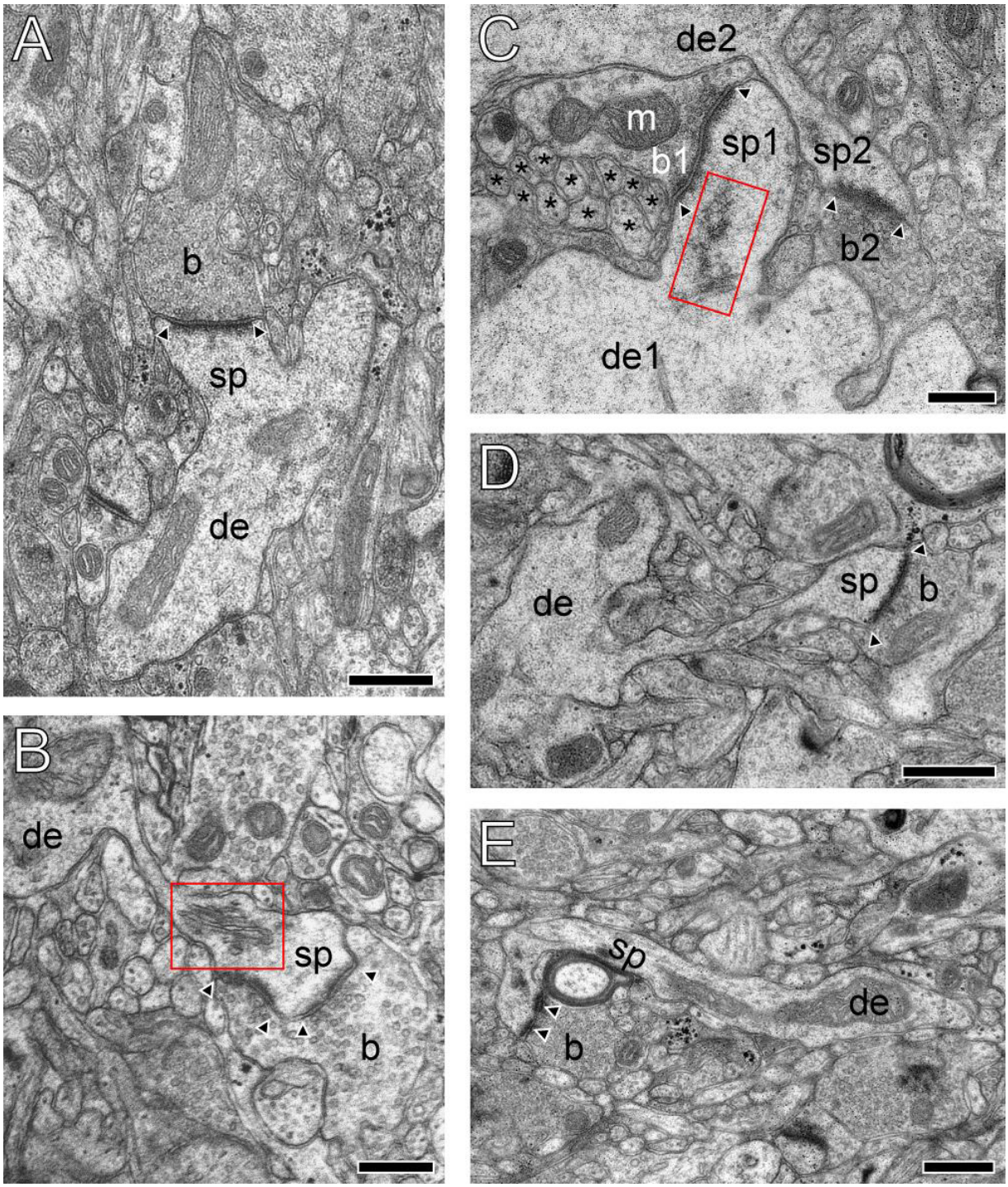

Figure 6: Diverse Types of Dendritic Spines

A) Large synaptic bouton (b) terminating on a typical stubby spine (sp) emerging from a dendrite (de). Arrowheads mark the AZ, covering almost the entire apposition zone. Scale bar 500nm. **B)** Synaptic bouton (b) established on an elongated mushroom spine (sp). Note the perforated appearance of the AZs (arrowheads). Red framed area marks a spine apparatus. Scale bar 250nm. **C)** Typical example of mushroom spine (sp1) connecting with a synaptic bouton (b1) including a mitochondrium (m). Another mushroom spine terminates on a second dendrite (de2). Arrowheads indicate AZ, red frame marks establishing spine apparatus. Note the unmyelinated axons (asterisk) between synaptic bouton b1 and dendrite de1. Scale bar 250nm. **D)** Rather small synaptic bouton (b) terminating on an elongated mushroom spine (sp). AZ covering entire apposition zone (arrowheads). Scale bar 500nm. **E)** Synaptic bouton (sp) terminates on long filopodial spine (sp) emerging from a dendrite (de). Scale bar 500nm.

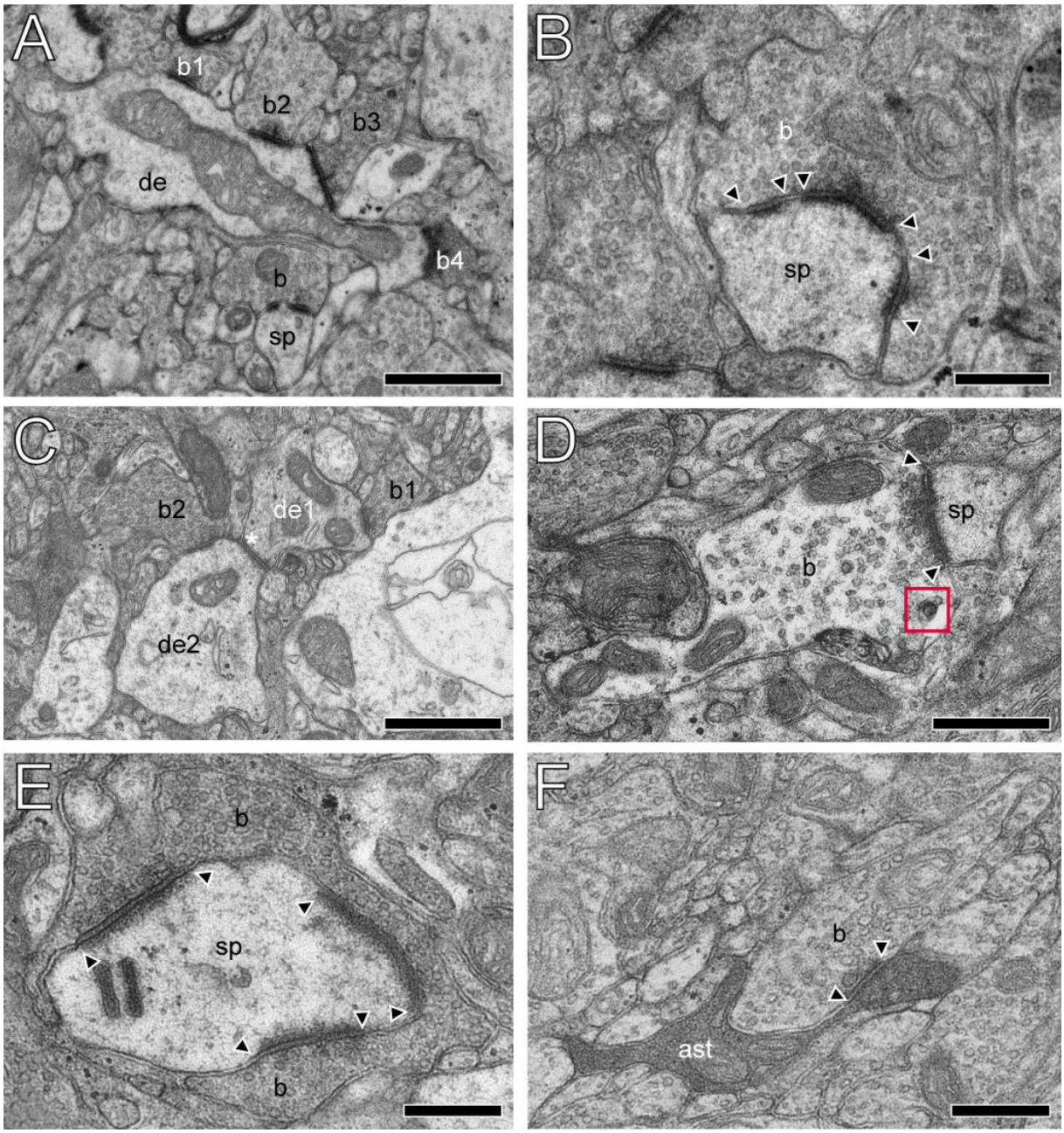

Figure 7: Synaptic Organization of Layer 1

A) Shaft synapses between four synaptic boutons (b1, b2, b3, b4) and one dendrite (de). Synaptic boutons b1 and b2 emerge rather small AZ, while AZs of synaptic boutons b3 and b4 cover entire apposition zone. Nearby synaptic bouton (b) terminates on a mushroom spine (sp) with perforated AZ. Scale bar 500nm. **B)** Large synaptic bouton (b) with perforated AZ (arrowheads) emerges on a typical mushroom spine (sp). Scale bar 250nm. **C)** Synaptic bouton (b1) terminates on a dendrite (de1) and another synaptic bouton (b2) establishes a synaptic contact on dendrite (de2). Note the dendro-dendritic synapse (asterisk) between neighboring dendrites (de1 and de2) indicated by the synaptic cleft. Scale bar 500nm. **D)** GABAergic (inhibitory) synaptic bouton (b) terminating on a spine (sp). AZ (arrowheads) covers complete apposition zone. Note the dense-core vesicle (red framed area) close to the synaptic cleft. Scale bar 250nm. **E)** Dendritic mushroom spine (sp) almost completely surrounded by synaptic bouton (b) terminating three large AZs. Note the clearly seen junction between membrane of synaptic terminal (b) and membrane of spine (sp). High vesicle concentration around AZs is a typical characterization for exhibitory synapses (Note the contrast to GABAergic synaptic bouton in D). Scale bar 250nm. **F)** Synaptic contact between astrocyte (ast) and synaptic bouton (b). Arrowheads mark the active zone. Scale bar 250nm.

3.3 Quantitative Analysis of Structural Synaptic Parameters of Layer 1

Beside the qualitative description of the neuronal and synaptic organization of L1 in the human TL neocortex, the second and more important part of this thesis was the definition, reconstruction and quantitative analysis of morphological parameters that represent structural correlates for synaptic transmission and plasticity (also see Chapter 2.3-2.5).

These parameters are:

1) the surface and volume of synaptic boutons

2) the surface and volume of mitochondria in the presynaptic terminal

3) the number and diameter of clear synaptic vesicles

4) the number and diameter of dense core vesicles

It has to be noted that the thorough analysis of two further important structural parameters, namely the size of the active zone and the three pools of synaptic vesicles were not included in this work (see Chapter 2.4). The quantification of active zones has to be done separately for the pre- and postsynaptic density, which is time- and labor-consuming and requires an exact outline of both membrane specializations in the stacked images comprising the z-stack. Furthermore, as already mentioned earlier, the definition of the three types of vesicle pools requires the measurement of the distance of each synaptic vesicle to the presynaptic density. This work is in progress and an important part of the doctoral thesis and the first publication.

The following Tables 3-6 show the summaries of structural parameters relevant for synaptic transmission and plasticity generated from the detailed 3D volume reconstructions with the software OpenCAR. As mentioned before, two areas of L1 in the human TL neocortex from two patients have been investigated. The first area (L1a) has been defined as closely located underneath the glia limitans (see Chapter 2.2 and 3.1), and is called L1a. The second area L1b comprises the area underneath L1a and the L1/2 border. To draw out possible morphological differences between areas and/or patients 15 boutons of each EM micrograph series have been reconstructed and data have been processed and summarized.

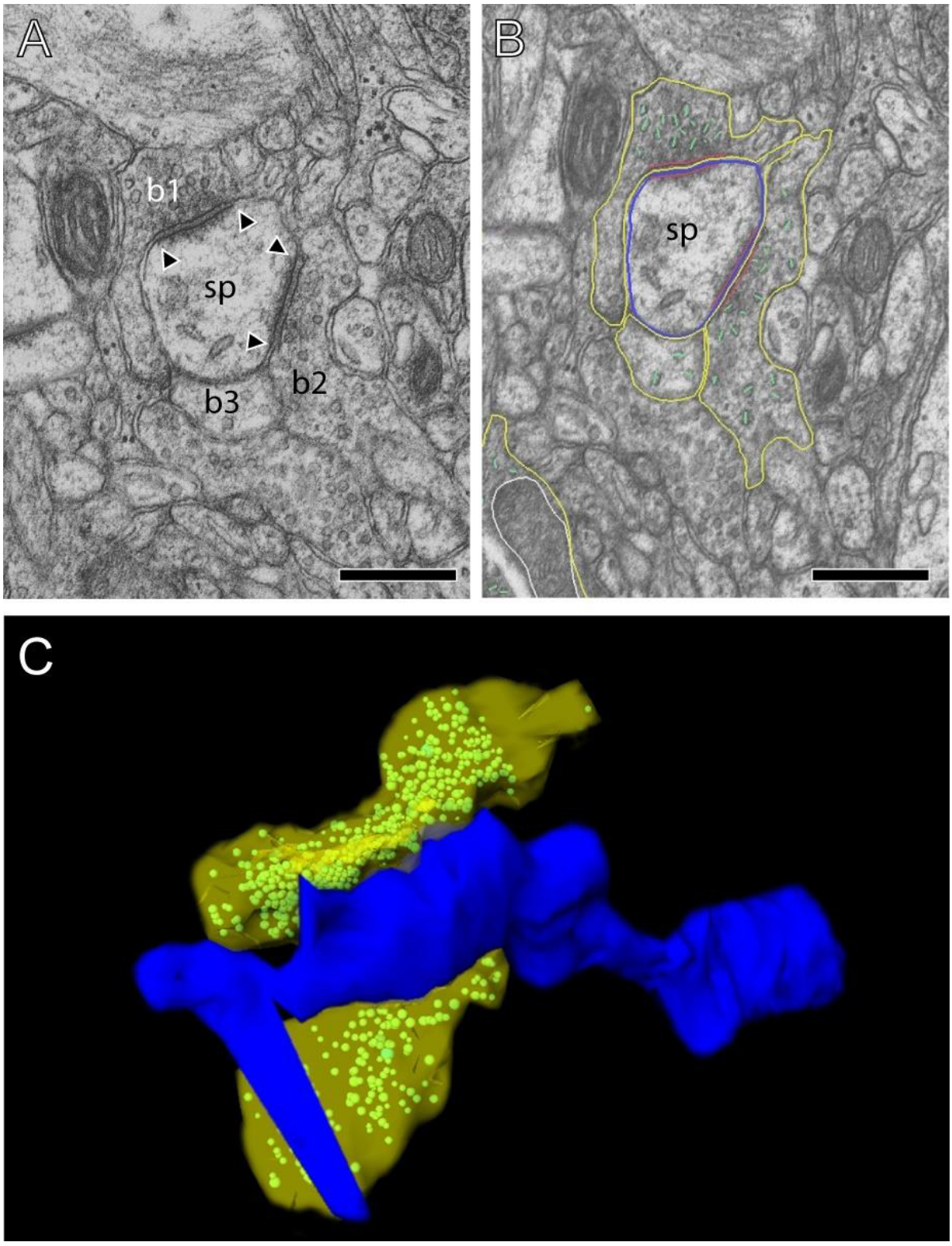

Figure 8: 3D Volume Reconstruction of two Synaptic Boutons in Layer 1

A) Consecutive EM micrograph of one spine (sp) with three surrounding synaptic boutons (b1, b2, b3). AZs are marked with arrowheads. Scale bar 250nm. **B)** Same image as in A. Synaptic boutons were outlined in yellow, spine in blue, pre- and postsynaptic densities of the spine in red, synaptic vesicles in green. Scale bar 250nm. **C)** Corresponding 3D volume reconstruction of the synaptic boutons b1 and b3 shown in A. Reconstruction of synaptic bouton b2 is not shown for reasons of better visibility. Color code: target spine in blue, synaptic bouton in transparent yellow and vesicles in green

3.3.1 QUANTITATIVE GEOMETRY OF SYNAPTIC BOUTONS

All analyzed and reconstructed boutons have established at least one synaptic contact with its postsynaptic target that could be a dendritic shaft of different caliber or a dendritic spine. The majority of the analyzed synaptic boutons contacted spines of different shape and size, the remainder dendrites. The following Table 3 shows the great variability with respect to surface area and volume of the individual synaptic boutons as indicated by the mean ± standard deviation (SD) regardless of their target structure. The range in shape and size of synaptic boutons reached from small 1.21µm²/0.05µm³ (L1b; HU_160217) to very large (with ~20-fold larger than the smallest measured synaptic bouton) 24.80µm²/2.93µm³ (L1a; HU_160217) synaptic boutons with a skew to medium-sized boutons.

Table 3: Quantitative Analysis of Layer 1 Synaptic Boutons
Summarized data of the size of synaptic boutons. Fifteen boutons of two regions in L1a and L1b of two patients have been reconstructed with OpenCAR and quantitatively analyzed.

		Synaptic Boutons		
Patient Identity	Region in L1	Total number of boutons	Surface ± SD [µm²]	Volume ± SD [µm³]
Patient 1 HU_160217	L1a	15	7.05 ± 5.63	0.58 ±0.70
	L1b	15	5.50 ± 2.78	0.39 ±0.23
Patient 2 HU_110204	L1a	15	5.65 ± 2.54	0.32 ±0.16
	L1b	15	6.19 ± 4.12	0.37 ±0.31
Mean ± SD (pooled)		60	6.10 ± 3.91	0.42 ± 0.41
Median (pooled)		60	5.13	0.34
CV (pooled)		60	0.64	0.98

3.3.2 QUANTITATIVE ANALYSIS OF MITOCHONDRIA

Mitochondria represent an important structural subelement in nerve terminals and serve distinct functions. First, as also in other organs (cells) of the body, they act as energy suppliers and are the main source in the production of adenosine-tri-phosphate. In nerve terminals they represent internal calcium stores and more important are involved in the regulation of the calcium homeostasis (Pozzan et al., 2000; Rizzuto et al., 2000). Calcium affects neuronal excitability, and is required e.g. for the supply and release of various neurotransmitters from synaptic vesicles, co-transmitters, neuropeptides, synaptic proteins (for example synaptophysin, -brevin, -tagmin) and other substances involved in synaptic transmission (reviewed by Südhof, 2012).

Table 4: Quantitative Analysis of Mitochondria of Layer 1 Synaptic Boutons
Summarized data of the size of mitochondria in synaptic boutons. A total of 60 boutons of two areas (L1a and L1b) of two patients have been reconstructed with OpenCAR and quantitatively analyzed.

		Mitochondria			
Patient Identity	Region in L1	Total number	Volume ± SD [µm³]	Number per bouton ± SD	Mean % of the volume of synaptic bouton
Patient 1 HU_160217	L1a	27	0.0187 ± 0.0183	1.80 ± 1.86	3.51 ± 3.28
	L1b	16	0.0145 ± 0.0199	1.07 ± 1.22	3.09 ± 4.23
Patient 2 HU_110204	L1a	19	0.0209 ± 0.0201	1.27 ± 0.88	5.88 ± 5.46
	L1b	13	0.0207 ± 0.0301	0.87 ± 1.25	4.29 ± 6.45
Mean ± SD (pooled)		75	0.0187 ± 0.0221	1.25 ± 1.36	4.19 ± 4.99
Median (pooled)		75	0.0146	1.00	2.71
CV (pooled)		75	1.18	1.09	1.19

Furthermore, mitochondria are highly mobile in nerve terminals and are found to be associated with the pool of synaptic vesicles (Mironov and Symonchuk, 2006). Moreover, it has been demonstrated that they are involved in the mobilization of synaptic vesicles from the resting pool (Verstreken et al., 2005; Perkins et al., 2010).

In this study, the number, shape and size of mitochondria varied widely in synaptic boutons. 21 (35%) out of 60 synaptic boutons had no mitochondria. The remainder were found to have at least a single up to six mitochondria (Figure 9A, B) occupying ~4% of the total synaptic bouton volume. The volume of mitochondria ranged from a minimum of 0.0055µm³ (L1a; HU_160217) to a maximum of 0.085µm³ (L1b; HU_110204). Interestingly small boutons contained no or only a single mitochondrium suggesting a correlation between boutons size and number of mitochondria.

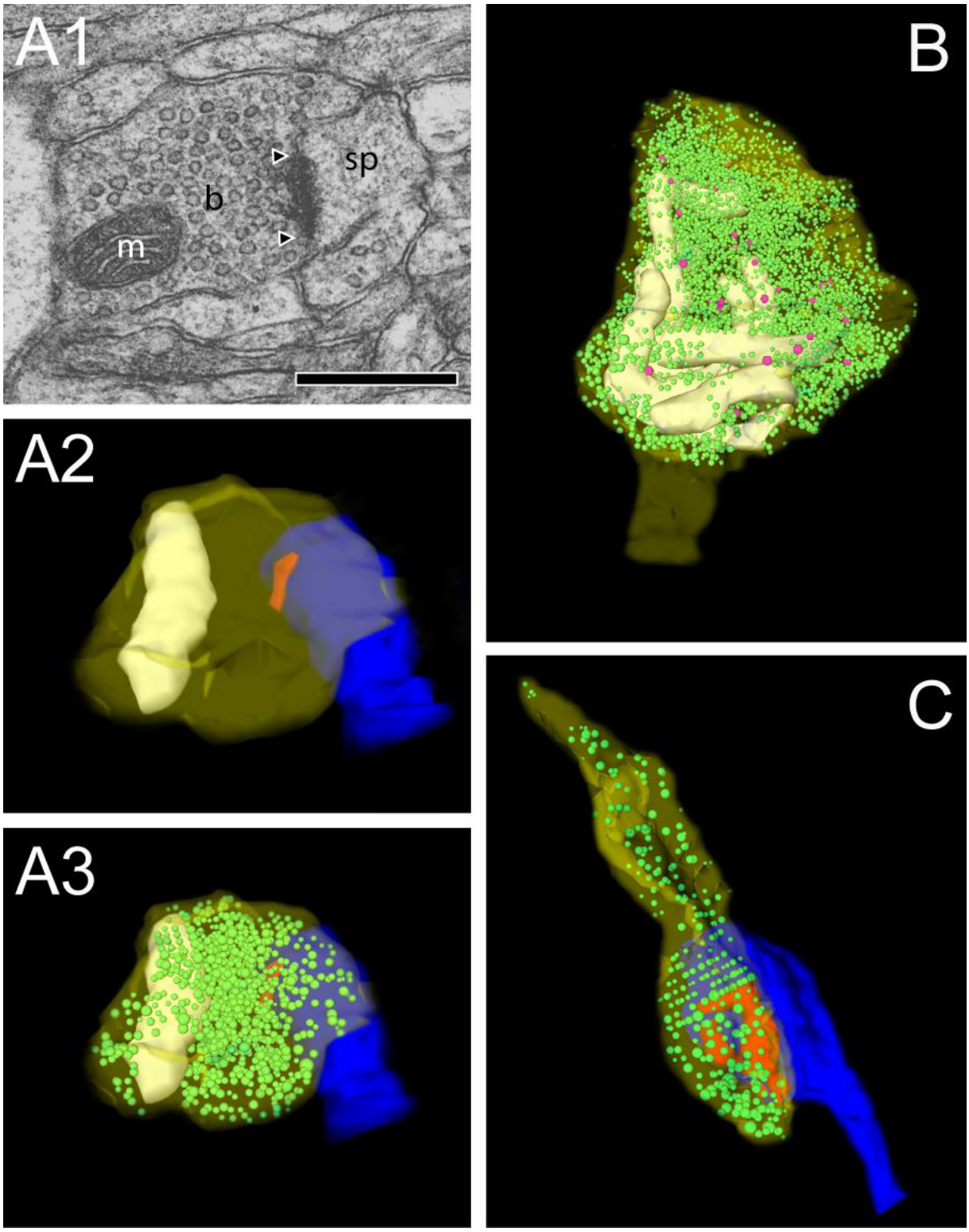

Figure 9: 3D Volume Reconstructions of Synaptic Structures in Layer 1

A1) High magnification electron micrograph of a synaptic bouton (b) containing a single mitochondrium (m) innervating a dendritic spine (sp). The AZ is marked by arrowheads. Scale bar 250nm. **A2-3)** Corresponding 3D volume reconstruction showing the synaptic bouton (transparent yellow), the AZ (red), the mitochondria (white) and the synaptic vesicles (green dots in A3). **B)** Synaptic bouton with a cluster of six mitochondria associated with synaptic and dense core vesicles. Color code as in A and dense core vesicle (magenta dots) **C**) 3D volume reconstruction shows a typical mushroom spine and a synaptic bouton with the AZ occupying most of the apposition zone. Color code as in A.

3.3.3 Shape and Size of Active Zones

The number, shape and size of AZs, composed of the pre- and postsynaptic density and the synaptic cleft are one of the main and hence critical determinants of synaptic transmission and plasticity. As already explained above, although the quantification of surface area and volume of the AZs is exceeding the scope of this master thesis, some qualitative observations can be made.

The majority of synaptic boutons (70%) had only a single AZ of different shape and size. Interestingly, in larger synaptic boutons three to four AZs were found (Figure 7E). Beside large AZs covering approximately the entire pre- and postsynaptic contact zone (Figure 6A, C D, 7C), also small AZs, spanning only approximately half or even less of the apposition zone were observed (Figure 8A1-A3). Perforations of either the pre- and postsynaptic density or both are frequently found among the population of analyzed synaptic boutons (Figure 7B, 10A-B). Nevertheless, also non-perforated continuous AZs were observed (Figure 10C, E).

3.3.4 Quantitative Analysis of the Total Pool of Synaptic Vesicles

Beside the AZ, the size and organization of the pool of synaptic vesicles is another key determinant involved in the synaptic transmission and the regulation (modulation) of synaptic plasticity (Schikorski, 2014; Watanabe, 2015; Rizzoli and Betz, 2005). In our analysis of synaptic boutons three major types of vesicles are observed. Small synaptic vesicles constituting the majority of synaptic vesicles (more than 80%) were distributed throughout the entire terminal (Figure 7A-B, E), but numerous were also found close or ‘docked’ to the presynaptic density. Larger clear synaptic vesicles were found either in close proximity to the presynaptic density (Figure 7F) or throughout the entire synaptic bouton. Finally, large dense core vesicles are found throughout the synaptic bouton (Figure 7D, 10A-E). In some cases, they were seen to fuse with the presynaptic density suggesting their involvement in the build-up of this membrane specialization.

The average number (mean) of synaptic vesicles over all analyzed boutons was 923.95 ± 761.53 (Table 5) with a minimum of 64 (L1a; HU_110204) and a maximum of 4988 (L1a; HU_160217) vesicles suggesting also a large RRP, RP and resting pool. Whether this is the case, will be investigated in further analysis.

The majority of synaptic boutons (~40%) contained a relatively large synaptic vesicle pool (see Table 5: median at 784 vesicles per bouton). The total pool of synaptic vesicles occupied ~3.5% of the total synaptic bouton volume and is smaller when compared with values of other CNS synapses (Rollenhagen et al., 2014).

Interestingly, no large variance in the diameter of the analyzed synaptic vesicles was found (28.72 ± 2.94nm) regardless of their distance to the presynaptic density.

Table 5: Quantitative Analysis of Vesicle Pool of Layer 1 Synaptic Boutons
Summarized data of structural parameters relevant for release of synaptic vesicles. Fifteen boutons of two regions in L1a and L1b of two patients have been reconstructed with OpenCAR and quantitatively analyzed.

		Synaptic Vesicles				
Patient Identity	Region in L1	Mean ± SD	Min	Max	Mean diameter ± SD [nm]	Mean % of the volume of synaptic bouton
Patient 1 HU_160217	L1a	1286.07 ± 1152.66	374	4988	27.12 ± 2.73	3.30 ± 0.76
	L1b	850.20 ± 621.45	261	2495	29.46 ± 4.00	3.46 ± 1.23
Patient 2 HU_110204	L1a	794.53 ± 402.48	64	1433	29.84 ± 2.18	4.12 ± 1.55
	L1b	765.00 ± 613.05	84	2218	28.47 ± 1.88	2.84 ± 1.00
Mean ± SD (pooled)		923.95 ± 761.53	64	4988	28.72 ± 2.94	3.43 ± 1.23
Median (pooled)		784.00			28.83	3.27
CV (pooled)		0.82			0.10	0.36

Dense core vesicles were observed in ~75% of the investigated boutons. Relatively large boutons seem to have more dense core vesicles (Maximum of 39 in L1a; HU_160217) than small synaptic boutons. Although the majority of the dense core vesicles were distributed throughout the entire synaptic bouton, some were found close the presynaptic density (Figure 7D). In Table 6 the determined structural parameters of dense core vesicles are shown. The average number of dense core vesicles in individual synaptic bouton was 4.30 ± 6.66. They were ~2-fold larger in diameter than synaptic vesicles, hence their volume is ~4-fold larger than an average synaptic vesicle.

Table 6: Quantitative Analysis of Dense Core Vesicles of Layer 1 Synaptic Boutons
Summarized data of structural parameters relevant for release of synaptic vesicles. Fifteen boutons of two regions in L1a and L1b of two patients have been reconstructed with OpenCAR and quantitatively analyzed.

		Synaptic Dense Core Vesicles				
Patient Identity	Region in L1	Mean ± SD	Min	Max	Mean diameter ± SD [nm]	Mean % of the volume of synaptic bouton
Patient 1 HU_160217	L1a	7.60 ± 9.62	1	39	55.90 ± 10.47	0.18 ± 0.15
	L1b	2.53 ± 3.07	0	10	38.08 ± 32.49	0.09 ± 0.10
Patient 2 HU_110204	L1a	2.33 ± 2.99	0	9	38.95 ± 34.27	0.17 ± 0.23
	L1b	4.73 ± 7.52	0	30	56.53 ± 23.77	0.19 ± 0.17
Mean ± SD (pooled)		4.30 ± 6.66	0	39	47.36 ± 27.73	0.16 ± 0.17
Median (pooled)		2.00			58.96	0.12
CV (pooled)		1.55			0.59	1.44

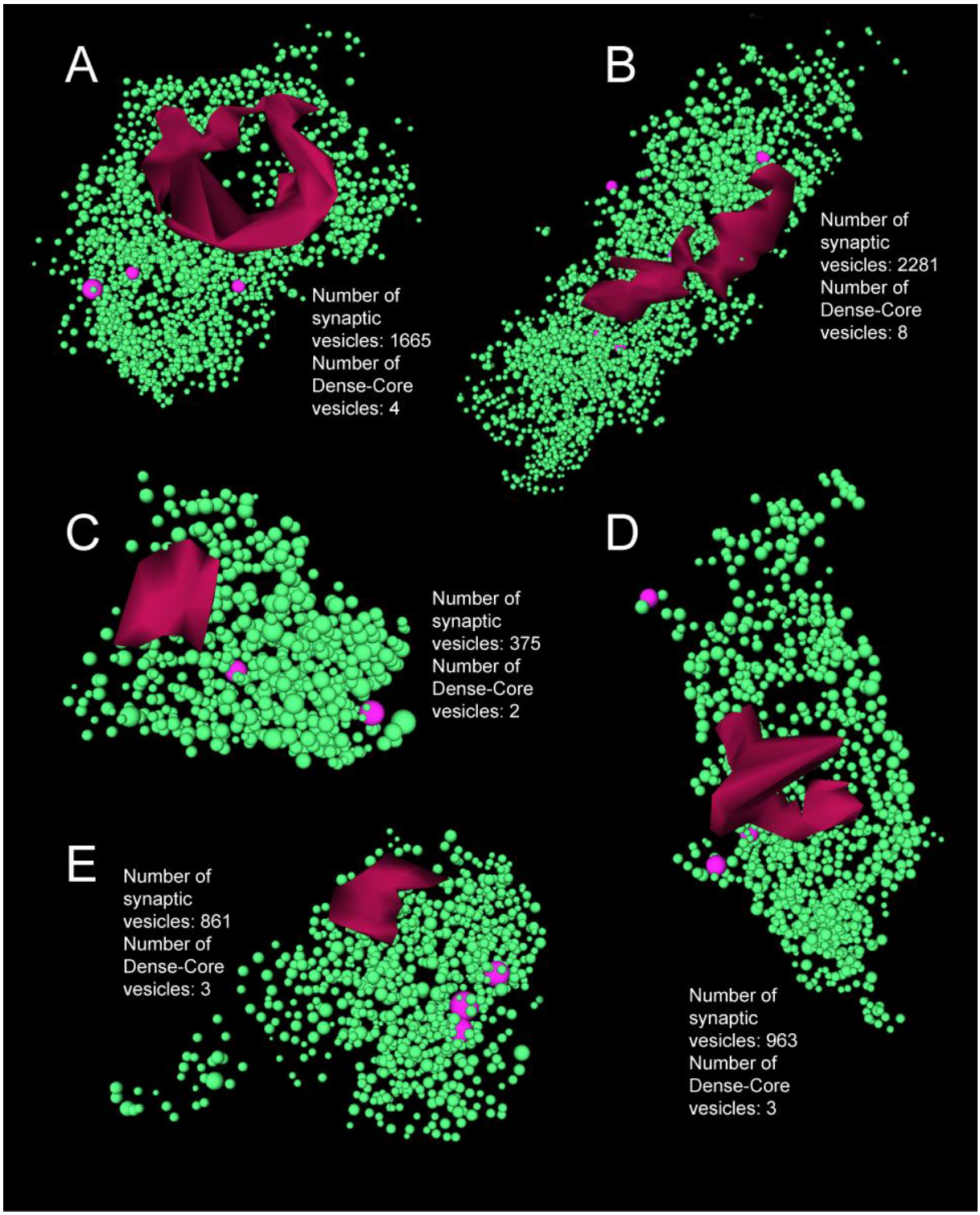

Figure 10: Pool of Synaptic Vesicles at individual Layer 1 Synaptic Boutons
A-E) Comparison of the total pool of synaptic vesicles (green dots) at AZs (red). The vesicle pools of individual synaptic boutons showed huge differences in the total pool size. Vesicles are homogenously distributed over the entire bouton and no cluster-like arrangements were observed. Dense core vesicles (magenta dots) have the double diameter of clear synaptic vesicles and were frequently observed intermingled with the pool of synaptic vesicles.

3.3.5 Statistical Analysis of the Structural Synaptic Parameters

To estimate possible statistical variances between the two analyzed areas in L1 and the two patients a box plot analysis was performed based on the quantitative data.

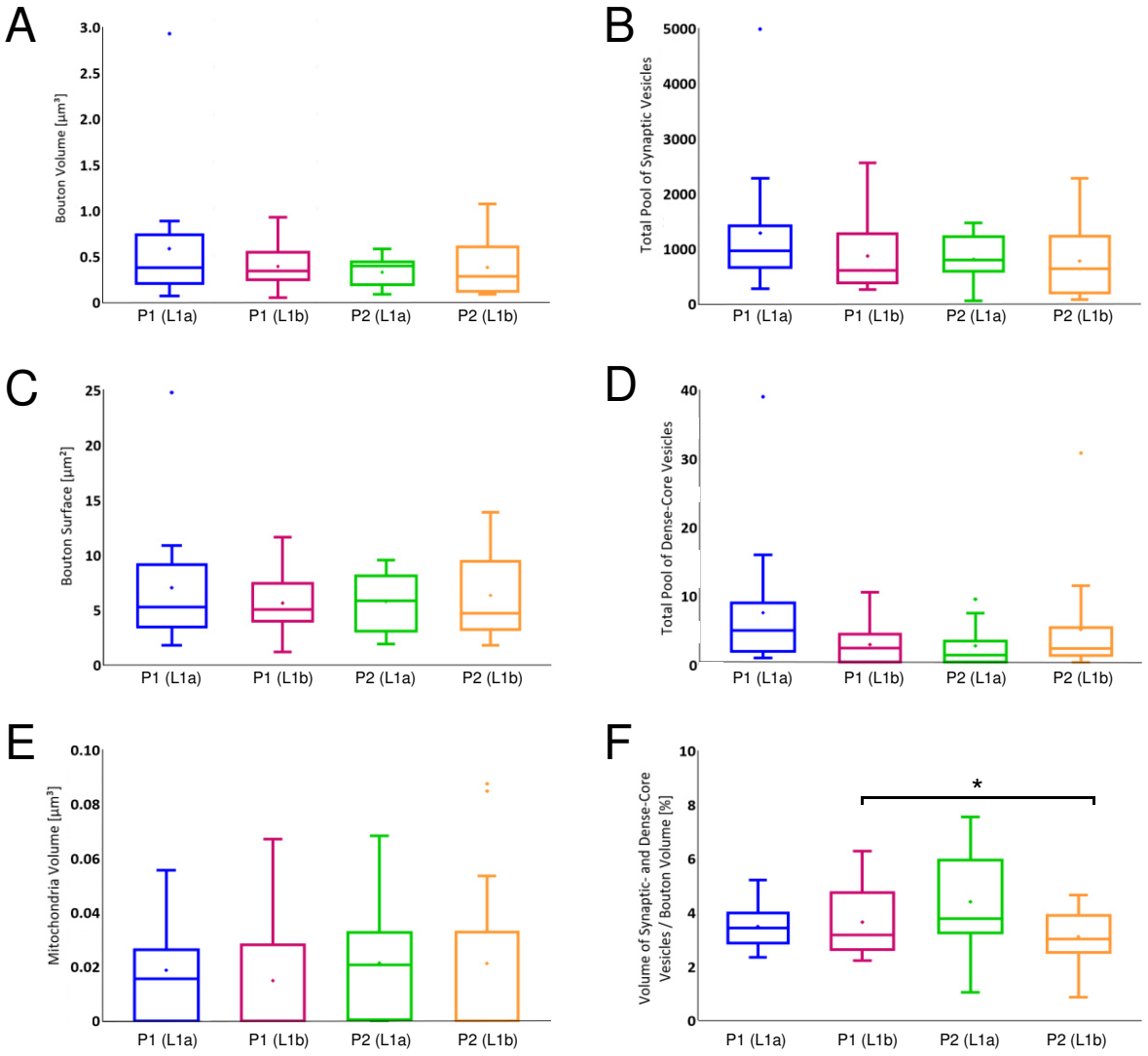

Figure 11: Box plots of various Structural Parameters of Layer 1 Synaptic Boutons
Data shown for structural parameters: volume (**A**) and surface (**B**) of boutons, volume of mitochondria (**E**), total pool of synaptic (**B**) and dense core (**D**) vesicles and percentage of synaptic and dense core vesicle volume of total bouton volume (**F**) over L1a and L1b of all patients. The data distributors are indicated by the medians (horizontal bars), IQRs (framed areas) and minimum and maximum (vertical lines). Points above the Maximum indicate outliner. Asterisk shows significance ($p<0.05$). For the structural parameters investigated no significant differences were observed despite the ratio of synaptic and dense core vesicle volume over bouton volume. P1 represents Patient 1 (HU_160217) and P2 represents Patient 2 (HU_110204).

The correlation of structural parameters between areas and patients with respect to the volume and surface area of boutons (Figure 11A, C), the volume of mitochondria (Figure 11E) and the total pool of synaptic and dense core vesicles (Figure 11B, D) showed no significant differences. According to this no difference in the structural composition of the defined L1a and L1b in the TL neocortex was observed. It has to be mentioned though that our sample size is too low to allow a final judgement. The only significance difference was found for the ratio of synaptic and dense core vesicle volume of the bouton volume (Figure 11F) between the two patients.

3.3.6 CORRELATIONS OF STRUCTURAL PARAMETERS

Finally, the determined structural parameters were tested for correlation. Therefore, all evaluated L1 synaptic boutons (n=60) were pooled. Dot plots from the investigated data were performed and a correlation coefficient (R^2) was calculated. The surface area of boutons is highly correlated to the volume of boutons (Figure 12A). The correlation coefficient of bouton volume over the total synaptic vesicle pool (R^2=0.92) was also strong (Figure 12D) indicating a direct relationship between the size of a synaptic bouton and the total pool of vesicles. In addition, a high correlation was found for the surface area of boutons and the total number of vesicles (R^2=0.87). Interestingly, the volume of boutons vs. the volume of mitochondria showed the weakest correlation (R^2=0.47). Thus, the volume of mitochondria seems to be independent from the size of the synaptic bouton, which may be explained by 35% of synaptic boutons lacking mitochondria.

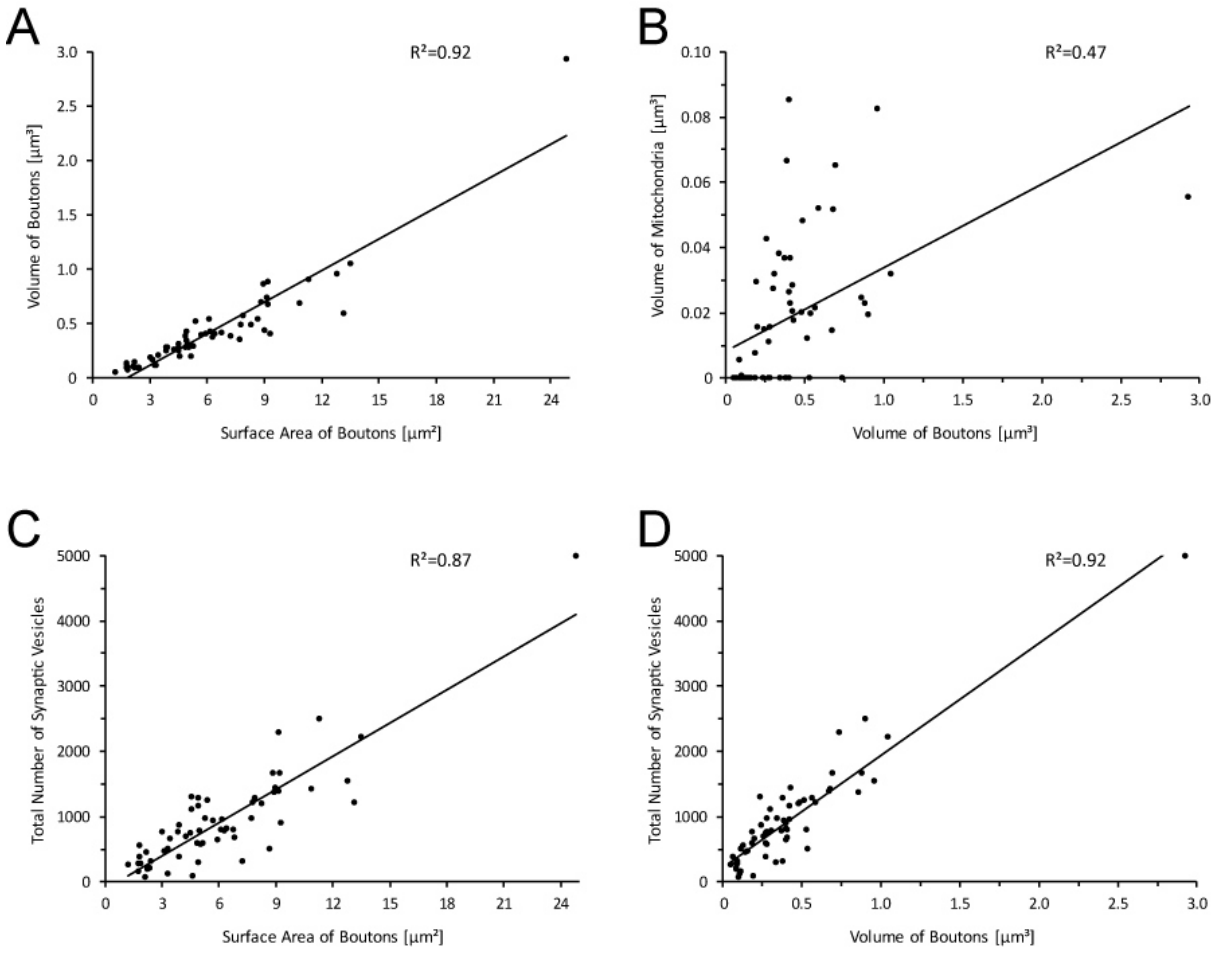

Figure 12: Correlation diagrams of Structural Parameters of Layer 1 Synaptic Boutons
Correlation diagrams between surface area vs. volume of bouton (**A**), volume of bouton vs. volume of mitochondria (**B**), surface area vs. total number of synaptic vesicles (**C**) and volume of boutons vs. total number of synaptic vesicles (**D**). Data points were all fitted for linear regression. The correlation coefficients (R^2) are shown at the corresponding graphs.

4 DISCUSSION

The present study is the first comprehensive quantification of synaptic boutons located in L1 of the human TL neocortex. The synaptic boutons of L1 show some similarities but also differ substantially from those described in various animal species. Although synapses are composed of nearly the same structural subelements, it is likely that their individual and specific composition makes them unique entities, perfectly adapted to their function in the microcircuit, in which they are embedded.

4.1 METHODOLOGICAL CONSIDERATIONS

Numerous studies have already described certain aspects of the neocortical ultrastructure in humans using post-mortem healthy and/or pathologically altered brains (Cragg, 1976; Gibson, 1983; DeFelipe et al., 1999b; Roberts et al., 2005; Kirkpatrick et al., 2006; Alonso-Nanclares et al., 2008; Blazquez-Llorca et al., 2013; Kay et al., 2013; reviewed by Bernhardt et al., 2013; Liu and Schumann, 2014). However, the degree of tissue preservation and thus the associated loss in preserving the ultrastructure are the critical limitations. This is causally related to the required time window between the death, the opening and removal of the brain and its fixation, which leads to severe alterations in the ultrastructure in post-mortem brains. The most obvious ones are the structural appearance of the entire neuropil, e.g. of membranes, numerous cytoplasmic organelles and, most importantly, synaptic structures (AZs and synaptic vesicles). Consequently, the use of post-mortem tissue is not suitable for fine-scale investigations and the generation of quantitative 3D models of synaptic boutons and their target structures as achieved in this study (see also Blazquez-Llorca et al. 2013).

To overcome this problem, we have taken advantage of brain tissue provided directly from surgery of pharmaco-resistant epileptic patients (see Table 1), which was immediately immersion-fixed after its removal. Under these conditions, tissue fixation is only dependent on the diffusion (penetration) of the fixative over time alone, which can also vary from specimen to specimen. Best results were achieved by immersion-fixation of 24 to 48 hours. This approach produced excellent preservation of human brain tissue, as demonstrated here.

The suitability of biopsy material for structural investigations in humans has become attractive as demonstrated by recent studies quantitatively describing the dendritic and axonal architecture of individual pyramidal neurons across layers of adult human neocortex using acute brain slices combined with intracellular biocytin-fillings (Mohan et al., 2015). This approach was even extended to study synaptic connectivity between different types of cortical neurons (Schwartzkroin and Prince, 1978; Testa-Silva et al., 2010; Verhoog et al., 2013; Testa-Silva et al., 2014; Mohan et al., 2015; Molnár et al., 2016). Altogether, these studies, including ours, clearly demonstrate that biopsy samples taken from epilepsy/tumor surgery are well suited for structural and functional investigations in humans.

4.2 Structural Organization of Layer 1

In general, L1 in the adult neocortex is described as the most cell sparse of the six layers. This is supported by our findings in the human TL neocortex although the volume of L1 seems to be larger when compared with that in various animal species. Furthermore, a subdivision of L1 into sublaminae L1a (astrocytic and cellular domain) and L1b (dendritic and synaptic domain) is upon differences in the structural organization justified.

Overall, the structural composition of L1 in the human TL neocortex resembled that described for various animal species (Muralidhar et al., 2013). The vast majority are L1 GABAergic interneurons although their overall number is low compared with other cortical layers. However, several recent studies have demonstrated that L1 GABAergic interneurons show a great heterogeneity in morphological, biochemical and physiological characteristics (Wang et al., 2004a; Wozny and Williams, 2011; Muralidhar et al., 2013; Jiang et al., 2016; DeFelipe et al., 2013). It has been demonstrated that this heterogeneity is directly correlated to high-target specificity, different innervation pattern and hence providing different degrees in feedback and feedforward inhibition of L1 GABAergic interneurons. Although, interneurons are considered

to be short-axon neurons, they are also found to project into other cortical areas connecting L1 to different layers (Tomioka and Rockland, 2007). Whether GABAergic interneurons in L1 of the human neocortex are structurally and functionally as diverse as their counterparts in animal species remains largely unknown and has to be investigated.

Transient CR cells are among the first generated neurons in the neocortex and are important in cortico- and synaptogenesis (also see Chapter 1.2). With their axons, they form a dense and long-range horizontal network with a high density of synaptic boutons along their axonal collaterals and innervate shafts and spines of terminal dendrites of pyramidal neurons (Anstötz et al., 2014). For most species the total disappearance of CR cells by apoptosis after the development of the neocortex is reported (Marín Padilla, 2001; Chowdhury et al., 2010). A striking difference to animal species is that in the human L1 numerous CR cells survive (Figure 5A-B) and do not undergo caspase-3 driven cell death. Interestingly, several CR cells also contained so-called lipofuscin granula (Figure 5A, B) typical for aging neurons which may point to a probable disappearance of these CR cells over time in humans. Whether CR cell in humans are embedded in the L1 circuitry is unknown due to the lack of structural data, in particular that of their axons. Interestingly, so far no synaptic input could be identified on human CR cells in our material, a prerequisite for a neuron to be embedded in a given microcircuit. Whether CR cells in humans survive while they undergo selective cell death in animal species remains unknown and has to be further investigated. It has been postulated though that CR cells actively participate in the physiology of the brain and possible consequences of their dysfunction on the pathology of the nervous system have only been emphasized.

A dense network of astrocytes is present in L1 of the human TL neocortex. Numerous studies have revealed the impact of astrocytes on synaptic transmission (Bergles et al., 2000; Lin et al., 2007; reviewed by Chung et al., 2015) by regulation of the brain homeostasis (Simard and Nedergaard, 2004). They redistribute the excess of extracellular potassium (K^+) during high neuronal activity (Chever et al., 2010; Bay and Butt, 2012) and control the temporal and spatial concentration of glutamate within the synaptic cleft (Rollenhagen et al., 2014) by a tight ensheathment of synaptic complexes and fine astrocytic processes that reach as far as the synaptic cleft. Hence astrocytes prevent synaptic cross talk by the active uptake of horizontally diffused glutamate via glutamate transporters thereby modulating the postsynaptic response. Moreover, it was demonstrated that calcium signals in astrocytes can be triggered by neural activity and astrocytic calcium signals can further promote neuronal response (Verkhratsky and

Kettenmann, 1996). Preliminary own results demonstrate also a close relationship between astrocytes, synaptic boutons and dendrites in L1, but this has to be further investigated.

In this thesis L1 has been subdivided into L1a and L1b to prove possible structural differences by qualitative and quantitative analysis. As described above, some similarities but also differences in the structural composition were found, while the quantitative analysis showed no significant differences with respect to synaptic bouton size, volume of mitochondria and the pool of synaptic vesicles (Figure 11). However, it has to be noted that our sample size is to date too low to support this statement. Further quantitative analysis will be performed to substantiate this statement.

4.3 Shape, Size and Composition of Synaptic Boutons

In this study, synaptic boutons of L1 of the human TL neocortex have been investigated concerning their shape, size and composition. On average, a synaptic bouton had a surface area of 6.10 ± 3.91µm² and a volume of 0.42 ± 0.41µm³, respectively.

It has to be noted that the standard deviation indicates a huge variance in the pool size of synaptic boutons. The smallest observed bouton has a surface of 1.21µm² and a volume of 0.05µm³, whereas the size and volume of the largest synaptic bouton was ~20fold larger with 24.80µm² and 2.93µm³. Despite the great variance, the correlation between surface and volume of synaptic boutons are strong (R^2=0.92).

Although the number of neurons in L1 of the cat visual cortex is 1173/mm³ compared to 100.000/mm³ in other layers (Gabbott and Somogyi, 1986), the high connectivity to other layers has been demonstrated (Chu and Hablitz, 2003; Larsen and Callaway, 2006; Oberlaender et al., 2011; Wozny and Williams, 2011) making L1 to a highly integrated part of the cortical network. Therefore, a detailed quantitative analysis of L1 synaptic boutons is required to compare them with those of other cortical layers.

The observed L1 boutons are medium-sized and similar in size to boutons described for L4 and L5 of the ‘barrel’ field in the adult rat and mouse somatosensory and motor cortex (Rollenhagen et al., 2014; Bopp et al., 2017; Hsu et al., 2017) but somewhat larger than those described for the CA1 subregion of the hippocampus (Harris and Sultan, 1995; Schikorski and Stevens, 2001; Marrone et al., 2005).

No comparable coherent studies of synaptic boutons of L1 in the human neocortex were found. However, a comparison with quantitative data obtained in L2/3 (Hesse et. al., in preparation) and L5 (Yakoubi et al., submitted for publication) shows similarities of synaptic boutons with respect to surface and size for different cortical layers in the human TL neocortex.

Interestingly, the majority of synaptic contacts analyzed were established on dendritic spines of different shape and size, including stubby, mushroom and elongated filopodial spines (see Chapter 3). This seems to be a characteristic feature of the human neocortex because these observations are in good agreement with findings of our group in L2/3 and L5 of the human neocortex. The preference of synaptic boutons in targeting spines rather than dendrites may represent a highly target-specific innervation of terminal tuft dendrites representing an important calcium domain at pyramidal neurons. A dense innervation of spines through excitatory, glutamatergic synapses may play a significant role in the induction and spread of calcium-induced signaling taking place in L1. Additionally, it has been shown that terminal tuft dendrites of L2/3 and L5 pyramidal neurons that span several cortical columns are the Ca^{2+} spike initiation zone that interacts with the Na^{+} action potential initiation zone in the axon of the same neurons. This interaction might control regenerative potentials critical for the integration and amplification of sensory and modulatory inputs (Larkum et al., 1999; Larkum and Zhu, 2002; Jiang et al., 2014; Anstötz et al., 2014). This may result in an integrated synaptic activity in pyramidal cells by the activation of Ca^{2+} spikes in pyramidal cells via L1 synaptic boutons in and across cortical columns.

Furthermore, 65% of all synaptic boutons contained a minimum of one mitochondrium occupying an average volume of 4.19 ± 4.99% of the total synaptic bouton volume. A value that is comparably smaller by 2-3-fold as in L4 and L5 synaptic boutons (Rollenhagen et al., Yakoubi et al., manuscripts submitted for publication). When present mitochondria are arranged in clusters and always associated with the pool of synaptic vesicles as demonstrated for a number of CNS synapses. Mitochondria were reported to be highly mobile (Mironov and Symonchuk, 2006) and involved in the mobilization of vesicles from the resting pool (Verstreken et al., 2005; Rollenhagen et al., 2014).

The structural variability as indicated by the geometry of synaptic terminals, the establishment of synaptic contacts on spines of diverse types and the presence of mitochondria might suggest a high synaptic reliability, strength and plasticity at human L1 synaptic boutons.

4.4 Shape, Size and other Structural Features of Active Zones

Besides the size and shape of synaptic boutons also the structural composition of AZ plays an important role in the synaptic transmission and in modulating synaptic plasticity (Matz et al., 2010; Holderith et al., 2012). The majority of the investigated synaptic boutons (~70%) displayed a single, ~23% two and the remainder three to four AZs. Recent studies for other cortical synapses (Rollenhagen et al., 2014) as well as findings of other layers of the human neocortex (Yakoubi et al., submitted for publication; Hesse et al., in preparation) reported a similar distribution pattern. Beside very large AZs covering the entire apposition zone also rather small AZs have been observed. This variability of size has also been reported in several synapses of the CNS (reviewed by Rollenhagen and Lübke, 2006).

The size and shape of AZs are directly correlated with the size of the RRP and release probability (Matz et al., 2010; Freche et al., 2011; Holderith et al., 2012). Larger AZs had a higher release probability, a larger RRP and an increased number of calcium channels at the presynaptic density (Holderith et al., 2012). Another assumption is the correlation between perforations (periodic interruptions) of the postsynaptic density (PSD) with a higher synaptic efficacy (Geinisman et al., 1991; 1993). Furthermore, perforated PSDs had significant larger amounts of docked vesicles than unperforated PSDs (Nava et al., 2014) suggesting an increase in synaptic efficacy and strength. About 60% of all investigated AZs showed either a perforation in the pre- or postsynaptic density, or both. Whether such correlations also exist at L1 synaptic boutons needs to be further investigated.

4.5 Size and Organization of the Pool of Synaptic Vesicles

The size and organization of the total pool of synaptic vesicles is another critical determinant in synaptic efficacy, strength and plasticity (reviewed by Südhof, 2012). In this study an average number of 923.95 ± 761.33 synaptic vesicles per synaptic bouton, with a minimum of 64 and a maximum of ~5000 vesicles per bouton was counted. The extrema and the given standard deviation indicate a wide variability in the size of the total synaptic vesicle pool. As already discussed in Chapter 4.3 also the size of synaptic boutons was found occupying a broad range. Thus, the correlation coefficients between total number of synaptic vesicles and surface area (R^2=0.87) as well as the bouton volume (R^2=0.92) are important indicators for the proportional increase of the synaptic vesicle pool with the size of a synaptic bouton.

When compared with synaptic boutons of comparable size, for example in the rat 'barrel' cortex L4 (Rollenhagen et al., 2014) the vesicle pool of human L1 synaptic boutons is ~2fold larger. Another study in cortical L2/3 in humans demonstrated a similar large vesicle pool in line with our findings (Hesse et al., unpublished), while L5 synaptic boutons showed a larger total synaptic vesicle pool with 1518.52 ± 303.18 vesicles per bouton (Yakoubi et al., manuscript submitted). Nevertheless, all studies of synaptic vesicles in the human neocortex revealed nearly the same diameter of synaptic vesicles (~30nm) and dense core vesicles (~60nm) (Yakoubi et al., manuscript submitted; Hesse et al., unpublished).

The relative large total pool of synaptic vesicles also suggests comparably large RRPs, RPs and resting pools at L1 synaptic boutons and are thus an integral part of the PhD thesis.

5 OUTLOOK

This study is included in a series of ongoing research to investigate the structural, in particular the synaptic organization, of each cortical layer as exemplified for the temporal lobe human neocortex. The final aim is to directly compare findings obtained in different animal species with those of the human brain. In ongoing experiments, the number of reconstructed synaptic boutons will be increased to meet the requirements for a first publication. As already stated above a detailed analysis of the synaptic density in L1a and L1b, the quantification of the number, size and shape of the AZ, and the three synaptic vesicle pools, the RRP, RP and resting pool will be performed. Both parameters are critical determinants of synaptic transmission and plasticity. This lead to quantitative 3D models of synapses that can be used for numerical and/or Monte Carlo Simulations of various synaptic parameters that in humans are not accessible to experiment. In further studies, also a new generation of electron microscopes, a so-called Scanning-focus ion beam EM (FIB-SEM). This microscope allows the definition of a much larger ROI when compared with a standard transmission EM (TEM) and the generation of much larger z-stacks (up to 1000 images) as possible with ultrathin sectioning. The overall advantage of this technique is the sectioning (milling down to 10nm per step) of the specimen during image acquisition, resulting in a higher number of consecutive sections of a greater ROI with a nearly perfect alignment at a meanwhile qualitative high resolution. This increases the possibility to identify and analyze almost every synaptic bouton and its subelements in a given ROI and hence the implementation of a reference number, e.g. amount of synaptic contacts per unit of volume, to quantify the comparison of different layers and between species.

In the future, we will also concentrate on the molecular composition of the AZ, namely the density, distribution pattern and possible co-localization of neurotransmitter receptors and their subunits (postsynaptic) and the number and localization of Calcium domains (presynaptic) at human neocortical synapses. This will be achieved by a combination using high-sensitive single and multiple postimmunogold labeling on freeze fracture replica.

The aim is to better understand how synapses in different layers of the human neocortex contribute to the computational properties of cortical networks.

6 REFERENCES

Alonso-Nanclares L, Gonzalez-Soriano J, Rodriguez JR, DeFelipe J (2008) Gender differences in human cortical synaptic density. Proceedings of the National Academy of Sciences of the United States of America 105:14615–14619.

Anstötz M, Cosgrove KE, Hack I, Mugnaini E, Maccaferri G, Lübke JHR (2014) Morphology, input-output relations and synaptic connectivity of Cajal-Retzius cells in layer 1 of the developing neocortex of CXCR4-EGFP mice. Brain structure & function 219:2119–2139.

Bay V, Butt AM (2012) Relationship between glial potassium regulation and axon excitability: a role for glial Kir4.1 channels. Glia 60:651–660.

Bergles DE, Roberts JD, Somogyi P, Jahr CE (2000) Glutamatergic synapses on oligodendrocyte precursor cells in the hippocampus. Nature 405:187–191.

Bernhardt BC, Hong S, Bernasconi A, Bernasconi N (2013) Imaging structural and functional brain networks in temporal lobe epilepsy. Frontiers in human neuroscience 7:624.

Bielle F, Griveau A, Narboux-Nême N, Vigneau S, Sigrist M, Arber S, Wassef M, Pierani A (2005) Multiple origins of Cajal-Retzius cells at the borders of the developing pallium. Nature neuroscience 8:1002–1012.

Blazquez-Llorca L, Merchán-Pérez Á, Rodríguez J-R, Gascón J, DeFelipe J (2013) FIB/SEM technology and Alzheimer's disease: three-dimensional analysis of human cortical synapses. Journal of Alzheimer's disease : JAD 34:995–1013.

Bopp R, Holler-Rickauer S, Martin KAC, Schuhknecht GFP (2017) An Ultrastructural Study of the Thalamic Input to Layer 4 of Primary Motor and Primary Somatosensory Cortex in the Mouse. The Journal of neuroscience : the official journal of the Society for Neuroscience 37:2435–2448.

Cajal SR (1995) Histologie du système nerveux de l'homme et des vertébrés (1911). Histology of the nervous system of man and vertebrates (translated by N. Swanson and L.W. Swanson). New York: Oxford University Press.

Carlos JA de, Borrell J (2007) A historical reflection of the contributions of Cajal and Golgi to the foundations of neuroscience. Brain research reviews 55:8–16.

Chever O, Djukic B, McCarthy KD, Amzica F (2010) Implication of Kir4.1 channel in excess potassium clearance: an in vivo study on anesthetized glial-conditional Kir4.1 knock-out mice. The Journal of neuroscience : the official journal of the Society for Neuroscience 30:15769–15777.

Chicurel ME, Harris KM (1992) Three-dimensional analysis of the structure and composition of CA3 branched dendritic spines and their synaptic relationships with mossy fiber boutons in the rat hippocampus. The Journal of comparative neurology 325:169–182.

Chowdhury TG, Jimenez JC, Bomar JM, Cruz-Martin A, Cantle JP, Portera-Cailliau C (2010) Fate of cajal-retzius neurons in the postnatal mouse neocortex. Frontiers in neuroanatomy 4:10.

Chu Z, Hablitz JJ (2003) GABA(B) receptor-mediated heterosynaptic depression of excitatory synaptic transmission in rat frontal neocortex. Brain Research 959:39–49.

Chung WS, Allen NJ, Eroglu C (2015) Astrocytes Control Synapse Formation, Function, and Elimination. Cold Spring Harbor perspectives in biology 7:a020370.

Colonnier M (1968) Synaptic patterns on different cell types in the different laminae of the cat visual cortex. An electron microscope study. Brain Research 9:268–287.

Cragg BG (1976) Ultrastructural features of human cerebral cortex. Journal of anatomy 121:331–362.

D'Arcangelo G (2001) The role of the Reelin pathway in cortical development. Symposia of the Society for Experimental Biology:59–73.

DeFelipe J (2011) The evolution of the brain, the human nature of cortical circuits, and intellectual creativity. Frontiers in neuroanatomy 5:29.

DeFelipe J et al. (2013) New insights into the classification and nomenclature of cortical GABAergic interneurons. Nature reviews. Neuroscience 14:202–216.

DeFelipe J, Alonso-Nanclares L, Arellano JI (2002) Microstructure of the neocortex: comparative aspects. Journal of neurocytology 31:299–316.

DeFelipe J, González-Albo MC, Del Río MR, Elston GN (1999a) Distribution and patterns of connectivity of interneurons containing calbindin, calretinin, and parvalbumin in visual

areas of the occipital and temporal lobes of the macaque monkey. The Journal of comparative neurology 412:515–526.

DeFelipe J, Marco P, Busturia I, Merchán-Pérez A (1999b) Estimation of the number of synapses in the cerebral cortex: methodological considerations. Cerebral cortex (New York, N.Y. : 1991) 9:722–732.

Deller T, Korte M, Chabanis S, Drakew A, Schwegler H, Stefani GG, Zuniga A, Schwarz K, Bonhoeffer T, Zeller R, Frotscher M, Mundel P (2003) Synaptopodin-deficient mice lack a spine apparatus and show deficits in synaptic plasticity. Proceedings of the National Academy of Sciences of the United States of America 100:10494–10499.

Dufour A, Rollenhagen A, Sätzler K, Lübke JHR (2016) Development of Synaptic Boutons in Layer 4 of the Barrel Field of the Rat Somatosensory Cortex: A Quantitative Analysis. Cerebral cortex (New York, N.Y. : 1991) 26:838–854.

Economo Cv, Koskinas GN (1925) Atlas of cytoarchitectonics of the adult human cerebral cortex. Basel, Freiburg, Paris: Karger.

Elston GN, Benavides-Piccione R, DeFelipe J (2001) The pyramidal cell in cognition: a comparative study in human and monkey. The Journal of neuroscience : the official journal of the Society for Neuroscience 21:RC163.

Freche D, Pannasch U, Rouach N, Holcman D (2011) Synapse geometry and receptor dynamics modulate synaptic strength. PloS one 6:e25122.

Gabbott PL, Somogyi P (1986) Quantitative distribution of GABA-immunoreactive neurons in the visual cortex (area 17) of the cat. Experimental brain research 61:323–331.

Geinisman Y, deToledo-Morrell L, Morrell F (1991) Induction of long-term potentiation is associated with an increase in the number of axospinous synapses with segmented postsynaptic densities. Brain Research 566:77–88.

Geinisman Y, deToledo-Morrell L, Morrell F, Heller RE, Rossi M, Parshall RF (1993) Structural synaptic correlate of long-term potentiation: formation of axospinous synapses with multiple, completely partitioned transmission zones. Hippocampus 3:435–445.

Gibson PH (1983) EM study of the numbers of cortical synapses in the brains of ageing people and people with Alzheimer-type dementia. Acta neuropathologica 62:127–133.

Glickstein M (2014) Neuroscience. A Historical Introduction. Cambridge: The MIT Press.

Gray EG (1959) Axo-somatic and axo-dendritic synapses of the cerebral cortex: an electron microscope study. Journal of anatomy 93:420–433.

Harris KM, Stevens JK (1989) Dendritic spines of CA 1 pyramidal cells in the rat hippocampus: serial electron microscopy with reference to their biophysical characteristics. The Journal of neuroscience : the official journal of the Society for Neuroscience 9:2982–2997.

Harris KM, Sultan P (1995) Variation in the number, location and size of synaptic vesicles provides an anatomical basis for the nonuniform probability of release at hippocampal CA1 synapses. Neuropharmacology 34:1387–1395.

Hoffpauir BK, Pope BA, Spirou GA (2007) Serial sectioning and electron microscopy of large tissue volumes for 3D analysis and reconstruction. A case study of the calyx of Held. Nature protocols 2:9–22.

Holderith N, Lorincz A, Katona G, Rózsa B, Kulik A, Watanabe M, Nusser Z (2012) Release probability of hippocampal glutamatergic terminals scales with the size of the active zone. Nature neuroscience 15:988–997.

Horton JC, Adams DL (2005) The cortical column: a structure without a function. Philosophical transactions of the Royal Society of London. Series B, Biological sciences 360:837–862.

Hsu A, Luebke JI, Medalla M (2017) Comparative ultrastructural features of excitatory synapses in the visual and frontal cortices of the adult mouse and monkey. The Journal of comparative neurology 525:2175–2191.

Hubel DH, Wiesel TN (1963) Receptive fields of cells in striate cortex of very young, visually inexperimented kittens. Journal of neurophysiology 26:994–1002.

Jiang X, Lachance M, Rossignol E (2016) Involvement of cortical fast-spiking parvalbumin-positive basket cells in epilepsy. Progress in brain research 226:81–126.

Jiang X, Zhang JJ, Wang MY, Sui N (2014) Differential muscarinic modulation of synaptic transmission in dorsal and ventral regions of the rat nucleus accumbens core. Physiological research 63:135–142.

Kandel ER, Schwartz JH, Jessel TM, Siegelbaum SA, Hudspeth AJ, Mack S (2013) Principles of neural science. New York, Lisbon, London: McGraw-Hill Medical.

Kay KR, Smith C, Wright AK, Serrano-Pozo A, Pooler AM, Koffie R, Bastin ME, Bak TH, Abrahams S, Kopeikina KJ, McGuone D, Frosch MP, Gillingwater TH, Hyman BT, Spires-Jones TL (2013) Studying synapses in human brain with array tomography and electron microscopy. Nature protocols 8:1366–1380.

Kiernan JA (2011) Anatomy of the temporal lobe. Epilepsy research and treatment 2012:176157.

Kirkpatrick B, Xu L, Cascella N, Ozeki Y, Sawa A, Roberts RC (2006) DISC1 immunoreactivity at the light and ultrastructural level in the human neocortex. The Journal of comparative neurology 497:436–450.

Konur S, Yuste R (2004) Imaging the motility of dendritic protrusions and axon terminals: roles in axon sampling and synaptic competition. Molecular and cellular neurosciences 27:427–440.

Lampe PD, Lau AF (2004) The effects of connexin phosphorylation on gap junctional communication. The International Journal of Biochemistry & Cell Biology 36:1171–1186.

Larkum ME, Zhu JJ (2002) Signaling of layer 1 and whisker-evoked Ca2+ and Na+ action potentials in distal and terminal dendrites of rat neocortical pyramidal neurons in vitro and in vivo. The Journal of neuroscience : the official journal of the Society for Neuroscience 22:6991–7005.

Larkum ME, Zhu JJ, Sakmann B (1999) A new cellular mechanism for coupling inputs arriving at different cortical layers. Nature 398:338–341.

Larsen DD, Callaway EM (2006) Development of layer-specific axonal arborizations in mouse primary somatosensory cortex. The Journal of comparative neurology 494:398–414.

Lin D-T, Wu J, Holstein D, Upadhyay G, Rourk W, Muller E, Lechleiter JD (2007) Ca2+ signaling, mitochondria and sensitivity to oxidative stress in aging astrocytes. Neurobiology of aging 28:99–111.

Liu X-B, Schumann CM (2014) Optimization of electron microscopy for human brains with long-term fixation and fixed-frozen sections. Acta neuropathologica communications 2:42.

Lodato S, Arlotta P (2015) Generating neuronal diversity in the mammalian cerebral cortex. Annual review of cell and developmental biology 31:699–720.

Lodish H, Berk A, Kaiser CA, Krieger M, Bretscher A, Ploegh H, Amon A, Scott MP (2013) Molecular cell biology. New York, NY: Freeman and Company.

Lübke J, Feldmeyer D (2007) Excitatory signal flow and connectivity in a cortical column: focus on barrel cortex. Brain structure & function 212:3–17.

Lui JH, Hansen DV, Kriegstein AR (2011) Development and evolution of the human neocortex. Cell 146:18–36.

Luskin MB, Shatz CJ (1985) Studies of the earliest generated cells of the cat's visual cortex: cogeneration of subplate and marginal zones. The Journal of neuroscience : the official journal of the Society for Neuroscience 5:1062–1075.

Ma J, Yao X-H, Fu Y, Yu Y-C (2013) Development of layer 1 neurons in the mouse neocortex. Cerebral cortex (New York, N.Y. : 1991) 24:2604–2618.

Marín Padilla M (2001) Evolución de la estructura de la neocorteza del mamífero: nueva teoría citoarquitectónica. Revista de neurologia 33:843–853.

Marin-Padilla M (1975) Abnormal neuronal differentiation (functional maturation) in mental retardation. Birth defects original article series 11:133–153.

Marin-Padilla M, Marin-Padilla TM (1982) Origin, prenatal development and structural organization of layer I of the human cerebral (motor) cortex. Anatomy and Embryology 164:161–206.

Marrone DF, LeBoutillier JC, Petit TL (2005) Ultrastructural correlates of vesicular docking in the rat dentate gyrus. Neuroscience letters 378:92–97.

Matz J, Gilyan A, Kolar A, McCarvill T, Krueger SR (2010) Rapid structural alterations of the active zone lead to sustained changes in neurotransmitter release. Proceedings of the National Academy of Sciences of the United States of America 107:8836–8841.

Meyer G, González-Gómez M (2017) The Subpial Granular Layer and Transient Versus Persisting Cajal-Retzius Neurons of the Fetal Human Cortex. Cerebral cortex (New York, N.Y. : 1991):1–16.

Mironov SL, Symonchuk N (2006) ER vesicles and mitochondria move and communicate at synapses. Journal of cell science 119:4926–4934.

Mohan H, Verhoog MB, Doreswamy KK, Eyal G, Aardse R, Lodder BN, Goriounova NA, Asamoah B, B Brakspear ABC, Groot C, van der Sluis S, Testa-Silva G, Obermayer J, Boudewijns ZSRM, Narayanan RT, Baayen JC, Segev I, Mansvelder HD, Kock CPJ de (2015) Dendritic and Axonal Architecture of Individual Pyramidal Neurons across Layers of Adult Human Neocortex. Cerebral cortex (New York, N.Y. : 1991) 25:4839–4853.

Molnár G, Rózsa M, Baka J, Holderith N, Barzó P, Nusser Z, Tamás G (2016) Human pyramidal to interneuron synapses are mediated by multi-vesicular release and multiple docked vesicles. eLife 5.

Mountcastle VB, Davies PW, Berman AL (1957) Response properties of neurons of cat's somatic sensory cortex to peripheral stimuli. Journal of neurophysiology 20:374–407.

Mountcastle VB, Powell TP (1959) Central nervous mechanisms subserving position sense and kinesthesis. Bulletin of the Johns Hopkins Hospital 105:173–200.

Müller J, Reyes-Haro D, Pivneva T, Nolte C, Schaette R, Lübke J, Kettenmann H (2009) The principal neurons of the medial nucleus of the trapezoid body and NG2(+) glial cells receive coordinated excitatory synaptic input. The Journal of general physiology 134:115–127.

Muralidhar S, Wang Y, Markram H (2013) Synaptic and cellular organization of layer 1 of the developing rat somatosensory cortex. Frontiers in neuroanatomy 7:52.

Nava N, Chen F, Wegener G, Popoli M, Nyengaard JR (2014) A new efficient method for synaptic vesicle quantification reveals differences between medial prefrontal cortex perforated and nonperforated synapses. The Journal of comparative neurology 522:284–297.

Navarrete M, Perea G, Maglio L, Pastor J, García de Sola R, Araque A (2013) Astrocyte calcium signal and gliotransmission in human brain tissue. Cerebral cortex (New York, N.Y. : 1991) 23:1240–1246.

Neher E (2015) Merits and Limitations of Vesicle Pool Models in View of Heterogeneous Populations of Synaptic Vesicles. Neuron 87:1131–1142.

Nicol MJ, Walmsley B (2002) Ultrastructural basis of synaptic transmission between endbulbs of Held and bushy cells in the rat cochlear nucleus. The Journal of Physiology 539:713–723.

Noback CR, Demarest RJ, Ruggiero DA, Strominger NL (2005) The Human Nervous System. Structure and Function. Totowa, NJ: Humana Press Inc.

Oberlaender M, Boudewijns ZSRM, Kleele T, Mansvelder HD, Sakmann B, Kock CPJ de (2011) Three-dimensional axon morphologies of individual layer 5 neurons indicate cell type-specific intracortical pathways for whisker motion and touch. Proceedings of the National Academy of Sciences of the United States of America 108:4188–4193.

Ogawa M, Miyata T, Nakajima K, Mikoshiba K (1997) The action of reelin in the layering of cortical neurons in cerebrum. Tanpakushitsu kakusan koso. Protein, nucleic acid, enzyme 42:577–583.

Perkins GA, Tjong J, Brown JM, Poquiz PH, Scott RT, Kolson DR, Ellisman MH, Spirou GA (2010) The micro-architecture of mitochondria at active zones: electron tomography reveals novel anchoring scaffolds and cristae structured for high-rate metabolism. The Journal of neuroscience : the official journal of the Society for Neuroscience 30:1015–1026.

Pozzan T, Magalhães P, Rizzuto R (2000) The comeback of mitochondria to calcium signalling. Cell calcium 28:279–283.

Reynolds ES (1963) The use of lead citrate at high pH as an electron-opaque stain in electron microscopy. The Journal of cell biology 17:208–212.

Rizzoli SO, Betz WJ (2005) Synaptic vesicle pools. Nature reviews. Neuroscience 6:57–69.

Rizzuto R, Bernardi P, Pozzan T (2000) Mitochondria as all-round players of the calcium game. The Journal of Physiology 529:37–47.

Roberts RC, Xu L, Roche JK, Kirkpatrick B (2005) Ultrastructural localization of reelin in the cortex in post-mortem human brain. The Journal of comparative neurology 482:294–308.

Rollenhagen A, Klook K, Sätzler K, Qi G, Anstötz M, Feldmeyer D, Lübke JHR (2014) Structural determinants underlying the high efficacy of synaptic transmission and plasticity at synaptic boutons in layer 4 of the adult rat 'barrel cortex'. Brain structure & function 220:3185–3209.

Rollenhagen A, Lübke JHR (2010) The mossy fiber bouton: the "common" or the "unique" synapse? Frontiers in synaptic neuroscience 2:2.

Rollenhagen A, Sätzler K, Rodríguez EP, Jonas P, Frotscher M, Lübke JHR (2007) Structural determinants of transmission at large hippocampal mossy fiber synapses. The Journal of neuroscience : the official journal of the Society for Neuroscience 27:10434–10444.

Ronan L, Voets N, Rua C, Alexander-Bloch A, Hough M, Mackay C, Crow TJ, James A, Giedd JN, Fletcher PC (2014) Differential tangential expansion as a mechanism for cortical gyrification. Cerebral cortex (New York, N.Y. : 1991) 24:2219–2228.

Sätzler K, Söhl LF, Bollmann JH, Borst JG, Frotscher M, Sakmann B, Lübke JHR (2002) Three-Dimensional Reconstruction of a Calyx of Held and Its Postsynaptic Principal Neuron in the Medial Nucleus of the Trapezoid Body. The Journal of Neuroscience 22:10567–10579.

Schikorski T (2014) Readily releasable vesicles recycle at the active zone of hippocampal synapses. Proceedings of the National Academy of Sciences of the United States of America 111:5415–5420.

Schikorski T, Stevens CF (2001) Morphological correlates of functionally defined synaptic vesicle populations. Nature neuroscience 4:391–395.

Schwartzkroin PA, Prince DA (1978) Cellular and field potential properties of epileptogenic hippocampal slices. Brain Research 147:117–130.

Shatz CJ, Luskin MB (1986) The relationship between the geniculocortical afferents and their cortical target cells during development of the cat's primary visual cortex. The Journal of neuroscience : the official journal of the Society for Neuroscience 6:3655–3668.

Sikora MA, Gottesman J, Miller RF (2005) A computational model of the ribbon synapse. Journal of neuroscience methods 145:47–61.

Simard M, Nedergaard M (2004) The neurobiology of glia in the context of water and ion homeostasis. Neuroscience 129:877–896.

Südhof TC (2012) The presynaptic active zone. Neuron 75:11–25.

Testa-Silva G, Verhoog MB, Goriounova NA, Loebel A, Hjorth J, Baayen JC, Kock CPJ de, Mansvelder HD (2010) Human synapses show a wide temporal window for spike-timing-dependent plasticity. Frontiers in synaptic neuroscience 2:12.

Testa-Silva G, Verhoog MB, Linaro D, Kock CPJ de, Baayen JC, Meredith RM, Zeeuw CI de, Giugliano M, Mansvelder HD (2014) High bandwidth synaptic communication and frequency tracking in human neocortex. PLoS biology 12:e1002007.

Tomioka R, Rockland KS (2007) Long-distance corticocortical GABAergic neurons in the adult monkey white and gray matter. The Journal of comparative neurology 505:526–538.

Umeda T, Ebihara T, Okabe S (2005) Simultaneous observation of stably associated presynaptic varicosities and postsynaptic spines: morphological alterations of CA3-CA1 synapses in hippocampal slice cultures. Molecular and cellular neurosciences 28:264–274.

Verhoog MB, Goriounova NA, Obermayer J, Stroeder J, Hjorth JJJ, Testa-Silva G, Baayen JC, Kock CPJ de, Meredith RM, Mansvelder HD (2013) Mechanisms underlying the rules for associative plasticity at adult human neocortical synapses. The Journal of neuroscience : the official journal of the Society for Neuroscience 33:17197–17208.

Verkhratsky A, Kettenmann H (1996) Calcium signalling in glial cells. Trends in neurosciences 19:346–352.

Verstreken P, Ly CV, Venken KJT, Koh T-W, Zhou Y, Bellen HJ (2005) Synaptic mitochondria are critical for mobilization of reserve pool vesicles at Drosophila neuromuscular junctions. Neuron 47:365–378.

Wang X-J, Tegnér J, Constantinidis C, Goldman-Rakic PS (2004a) Division of labor among distinct subtypes of inhibitory neurons in a cortical microcircuit of working memory. Proceedings of the National Academy of Sciences of the United States of America 101:1368–1373.

Wang Y, Toledo-Rodriguez M, Gupta A, Wu C, Silberberg G, Luo J, Markram H (2004b) Anatomical, physiological and molecular properties of Martinotti cells in the somatosensory cortex of the juvenile rat. The Journal of Physiology 561:65–90.

Watanabe S (2015) Slow or fast? A tale of synaptic vesicle recycling. Science (New York, N.Y.) 350:46–47.

Wilke SA, Antonios JK, Bushong EA, Badkoobehi A, Malek E, Hwang M, Terada M, Ellisman MH, Ghosh A (2013) Deconstructing complexity. Serial block-face electron microscopic analysis of the hippocampal mossy fiber synapse. The Journal of neuroscience : the official journal of the Society for Neuroscience 33:507–522.

Wilson SM, Bacic A (2012) Preparation of plant cells for transmission electron microscopy to optimize immunogold labeling of carbohydrate and protein epitopes. Nature protocols 7:1716–1727.

Wimmer VC, Horstmann H, Groh A, Kuner T (2006) Donut-like topology of synaptic vesicles with a central cluster of mitochondria wrapped into membrane protrusions. A novel structure-function module of the adult calyx of Held. The Journal of neuroscience : the official journal of the Society for Neuroscience 26:109–116.

Wonders CP, Anderson SA (2006) The origin and specification of cortical interneurons. Nature reviews. Neuroscience 7:687–696.

Wozny C, Williams SR (2011) Specificity of synaptic connectivity between layer 1 inhibitory interneurons and layer 2/3 pyramidal neurons in the rat neocortex. Cerebral cortex (New York, N.Y. : 1991) 21:1818–1826.

Xu-Friedman MA, Harris KM, Regehr WG (2001) Three-Dimensional Comparison of Ultrastructural Characteristics at Depressing and Facilitating Synapses onto Cerebellar Purkinje Cells. The Journal of Neuroscience 21:6666–6672.

Xu-Friedman MA, Regehr WG (2003) Ultrastructural contributions to desensitization at cerebellar mossy fiber to granule cell synapses. The Journal of neuroscience : the official journal of the Society for Neuroscience 23:2182–2192.

Xu-Friedman MA, Regehr WG (2004) Structural contributions to short-term synaptic plasticity. Physiological reviews 84:69–85.

Zilles K, Bacha-Trams M, Palomero-Gallagher N, Amunts K, Friederici AD (2015) Common molecular basis of the sentence comprehension network revealed by neurotransmitter receptor fingerprints. Cortex; a journal devoted to the study of the nervous system and behavior 63:79–89.

SUMMARY

The mammalian brain consists of anatomically and functionally defined individual microcircuits and networks formed by neurons and their synapses. Synapses are the structural key element, not only connecting various neuronal cell types in different brain regions, nuclei or layers, for example in the cortical column, but more important are involved in the execution, modulation and termination of signal transduction between neurons. Hence synapses represent a major driving force in all cognitive processes of the human brain.

Since the announcement of the 'decade of the brain' nearly 20 years ago enormous efforts were made in the description of structural and functional characteristics of synapses in various brain regions and animals species using high-end electrophysiological, light- and electron microscopic and molecular techniques. However, our knowledge about the structural composition, in particular the synaptic organization of the human brain, is still comparably small. This can partially be attributed to the availability of human brain tissue for such sophisticated experiments. However, using access tissue from biopsy samples from pharmaco-resistant epileptic patients enabled us to perform a quantitative analysis of synaptic boutons in Layer 1 of the human temporal lobe neocortex. Serial ultrathin sections provided the basis for fine-scale electron microscopy and subsequent software supported 3D volume reconstruction of synaptic structures and finally, the generation of quantitative 3D models of synapses in Layer 1. Such models can then be used for direct comparison with other central nervous system synapses where quantitative data are available or for numerical simulations of various synaptic parameters not accessible to experiment in the human brain. Finally, this master thesis will contribute to the detailed description of the neuronal and synaptic organization of the human brain at the cellular, subcellular and molecular level of the human neocortex as exemplified for the temporal lobe neocortex that will be made accessible by our group.

In contrast to the underlying cortical layer, Layer 1 in the adult human brain is comparably cell sparse, but contained so-called Cajal-Retzius cells and GABAergic interneurons, as well as dendritic and synaptic structural elements and non-neuronal astrocytes and oligodendrocytes. Upon structural criteria Layer 1 can be subdivided into Layer 1a (astrocytic and cellular domain) and Layer 1b a more 'synaptic and dendritic domain'.

The majority of synaptic contacts were excitatory in nature and established on dendritic spines. Synaptic boutons varied substantially in surface area and volume, in the content of mitochondria and the total synaptic vesicle pool per bouton. Most synaptic terminals (70%) had a single neurotransmitter release site (active zone). The comparably large total pool of synaptic vesicles suggests also relatively large RRPs, RPs and resting pools.

In summary, our results demonstrate similarities but also distinct differences not only with synapses in other layers of the human temporal lobe neocortex but also with their counterparts in various animal species. Hence our findings will contribute to a fundamental and improved understanding of the 'behavior' of synapses embedded in cortical networks of the normal and pathologically altered brain.

LIST OF ABBREVIATIONS

3D	Three-Dimensional
AIS	Axon Initial Segment
AZ	Active Zone
CA1	Cornu Ammonis 1
CNS	Central Nervous System
CV	Coefficient of Variance
CR	Cajal-Retzius
EM	Electron Microscope
FIB-SEM	Focused Ion Beam Scanning Electron Microscope
GABA	Gamma-Aminobutyric Acid
IQR	Interquartile Range
L1	Layer 1
MRI	Magnetic Resonance Imaging
MZ	Marginal Zone
PB	Phosphate Buffer
PSD	Postsynaptic Density
ROI	Region of Interest
RRP	Readily Releasable Pool
RP	Recycling Pool
SD	Standard Deviation
SNARE	Soluble NSF Attachment Protein
TEM	Transmission Electron Microscope
TL	Temporal Lobe

LIST OF FIGURES

LIST OF TABLES

ACKNOWLEDGEMENTS

Firstly, I would like to express my sincere gratitude to my advisor Prof. Dr. Joachim Lübke for the continuous support, for his patience, motivation, and immense knowledge. His guidance helped me in all the time of research and writing of this thesis.

Besides my advisor, I would like to thank all members of the group 'Structure of Synapses' for the very good working atmosphere and encouraging support through the process of researching and writing this thesis.

Finally, I must express my very profound gratitude to my family and to my best friend for providing me with unfailing support and continuous encouragement throughout my years of study.

This accomplishment would not have been possible without you. Thank you.

ERKLÄRUNG

Ich erkläre, dass ich die vorliegende Arbeit selbstständig verfasst, andere als die angegebenen Quellen/Hilfsmittel nicht benutzt, und die den benutzten Quellen wörtlich und inhaltlich entnommenen Stellen als solche kenntlich gemacht habe.

Düsseldorf, am 31.08.2017 ……..

Julia Stöhr